nature catalysis

Supplementary information

https://doi.org/10.1038/s41929-024-01181-w

Localized thermal levering events drive spontaneous kinetic oscillations during CO oxidation on Rh/Al_2O_3

In the format provided by the authors and unedited

`

Table of Contents

`

`

Supplementary Methods

Sample Characterisation

Transmission electron microscopy

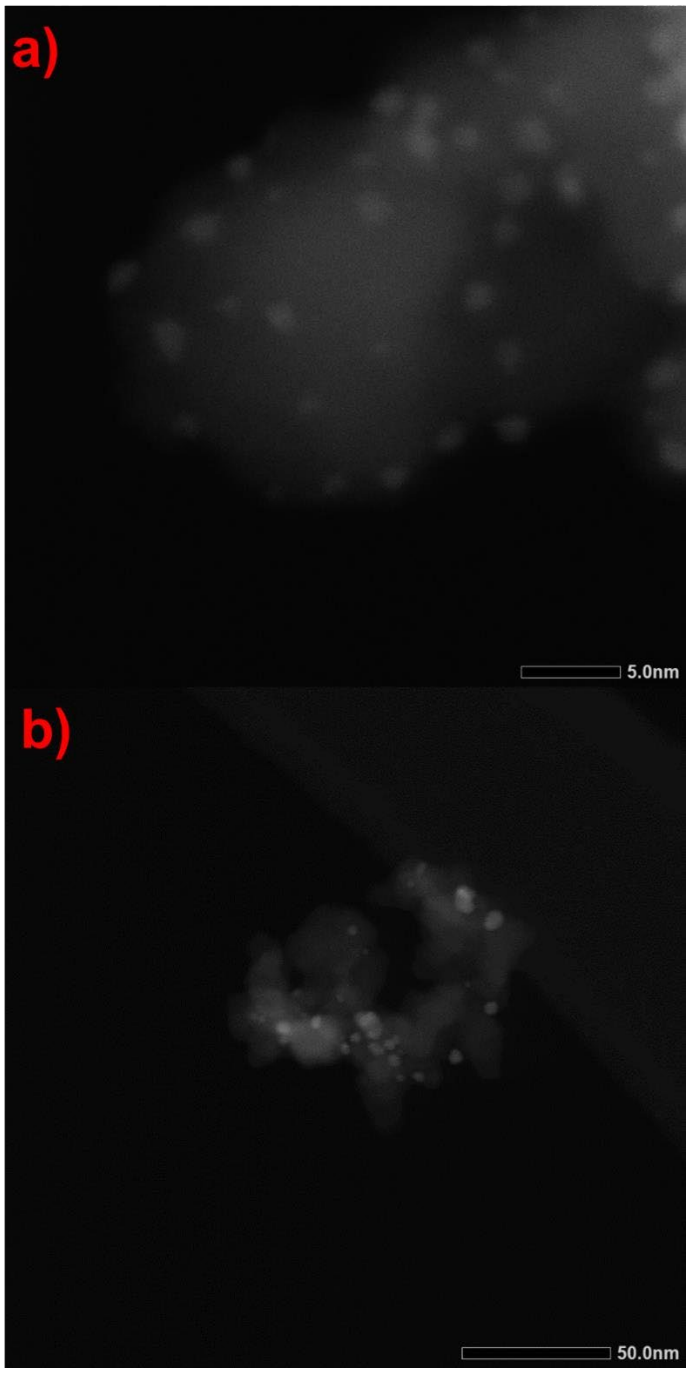

Supplementary Figure 1. Representative STEM-HAADF image of the Rh/Al2O3 catalyst in (a) the unused state and (b) the used state.

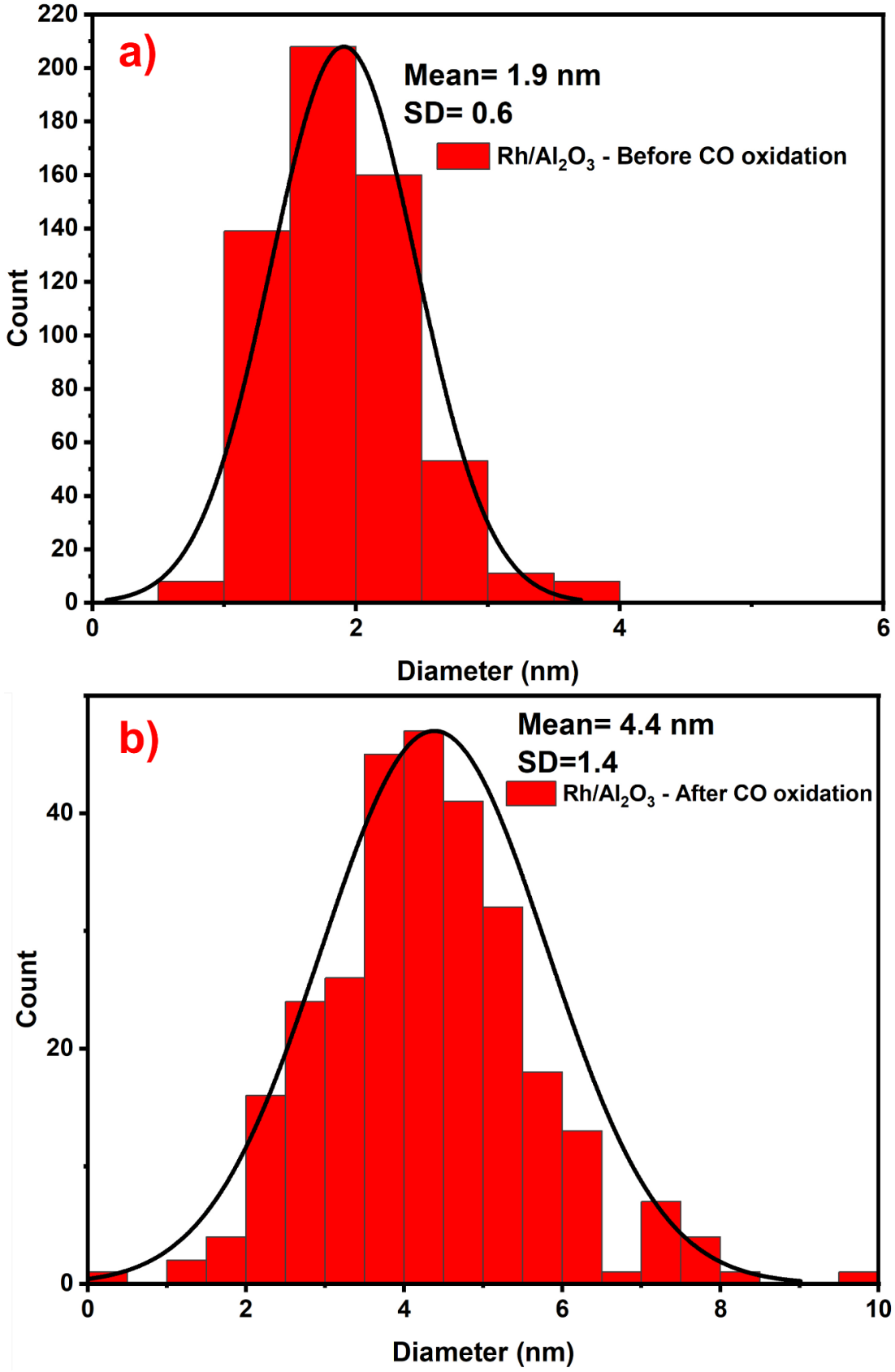

Supplementary Figure 2. Particle size distribution for Rh/Al_2O_3 in (a) the unused state and (b) the used state

`

Combined *operando* EDE/DRIFTS measurement

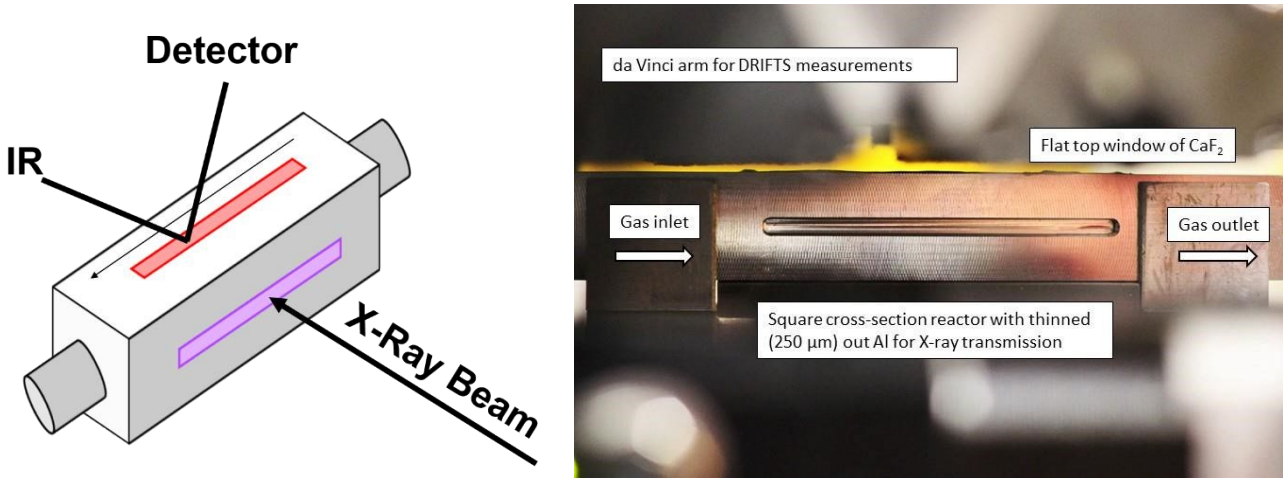

Supplementary Figure 3. (left panel) schematic of the cell used for the operando experiment, the area highlighted in red indicates the CaF_2 window, whereas the area highlighted in purple indicates the portion the aluminium reactor machined to 250µm. (right panel) front face photograph of the aluminium EDE/DRIFTS reaction cell.

`

Supplementary Discussion

Radiation damage evaluation

In order to check for any radiation damage, we dosed the sample for a total of 30 min and checked the intensity of the first XANES peak (the “white-line”). The first test shows a gradual increase in the white line of the oxidised Rh (S4-S5). Upon removal of water, through the use of a water trap positioned before the gas inlet, it is possible to see a drop to ~50% less radiation damage (S6-7). In order to further remove water, the sample was subject to the regeneration process required for the experiment, and subsequently cooled down and another radiation damage test was performed (S8-9), where a similar extent to radiation damage is observed, albeit in a different direction, reducing rather than oxidising. In order to reduce this effect, we have reduced the flux, at 23000 eV, to a cumulative transmission of 5.29 % (versus 18 mm gap and no extra attenuators in the beam). This was obtained by opening the gap to 27 mm + 25um Mo and + 10 um Pb. (the carbon attenuator, Be windows and Pt mirror are always in the beam at this energy). This reduced the beam damage to an extent which was deemed acceptable (Δ~0.07 a.u.) (S10-11). A new sample was put in the reactor and a similar behaviour could be observed, as shown in figure (S1215).

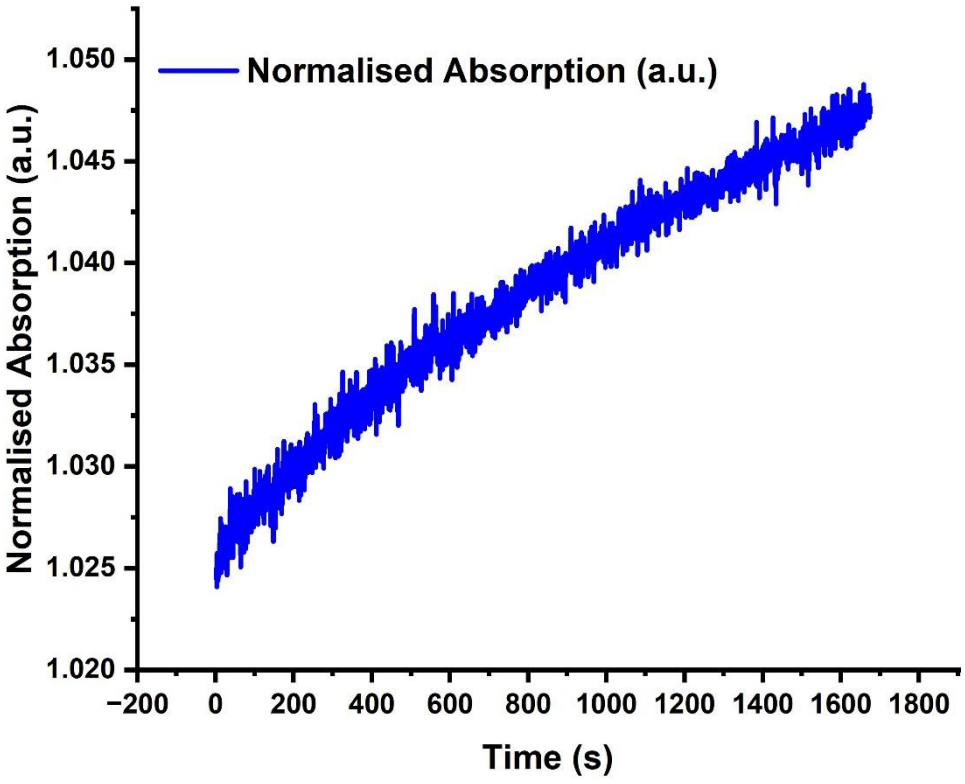

Supplementary Figure 4. Rh-K edge XANES trace as function of time under Ar at room temperature before radiative damage prevention.

`

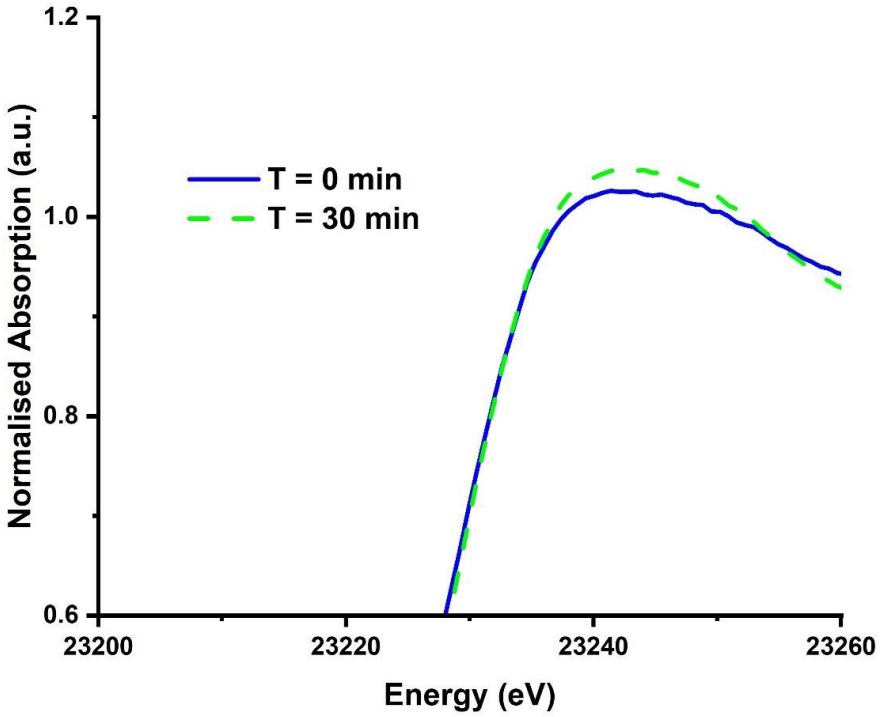

Supplementary Figure 5. Rh-K edge XANES spectra under Ar at 0 and 30 min before radiative damage prevention on a fresh sample.

`

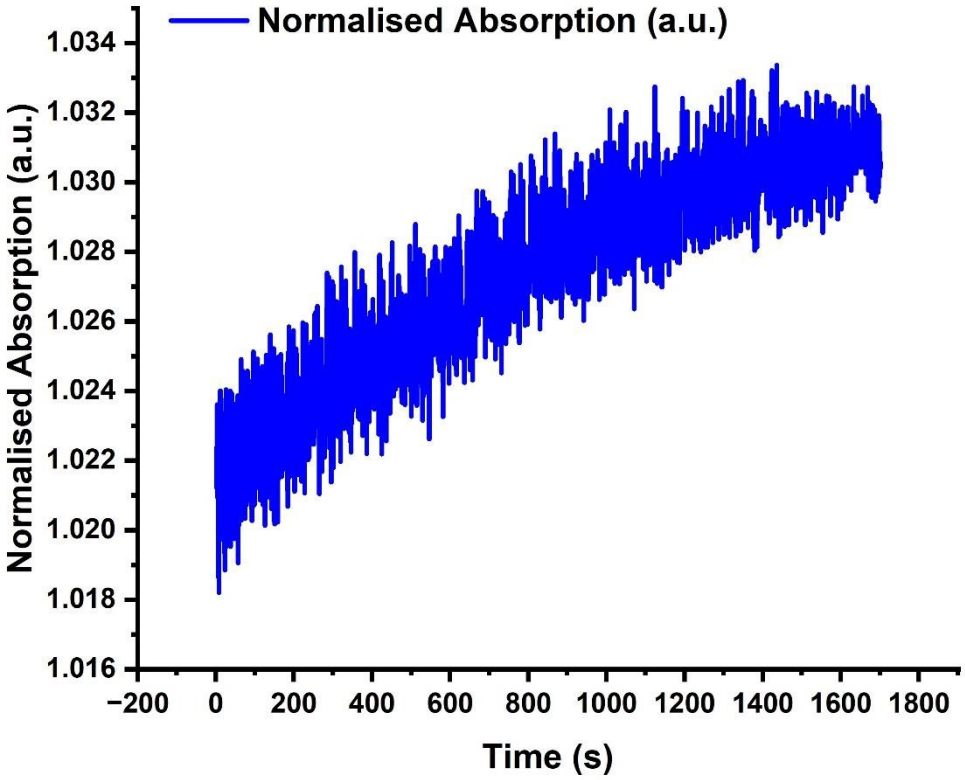

Supplementary Figure 6. Rh-K edge XANES trace as function of time under Ar at room temperature upon removal of water contribution.

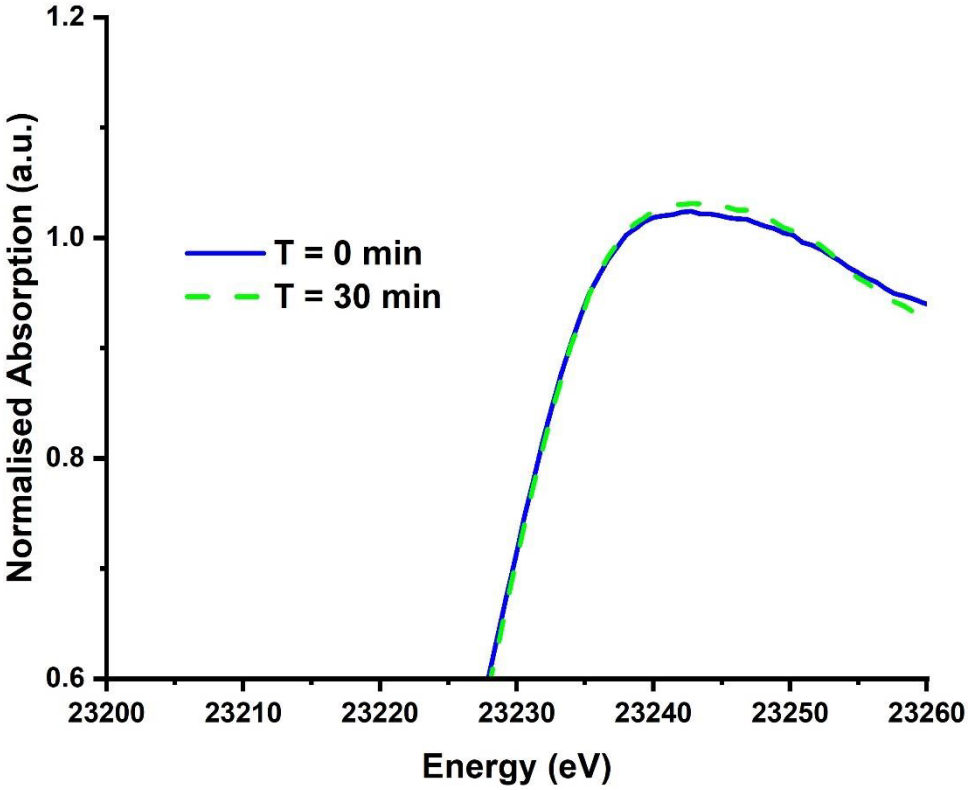

Supplementary Figure 7. Rh-K edge XANES spectra under Ar at 0 and 30 min upon removal of water contribution.

`

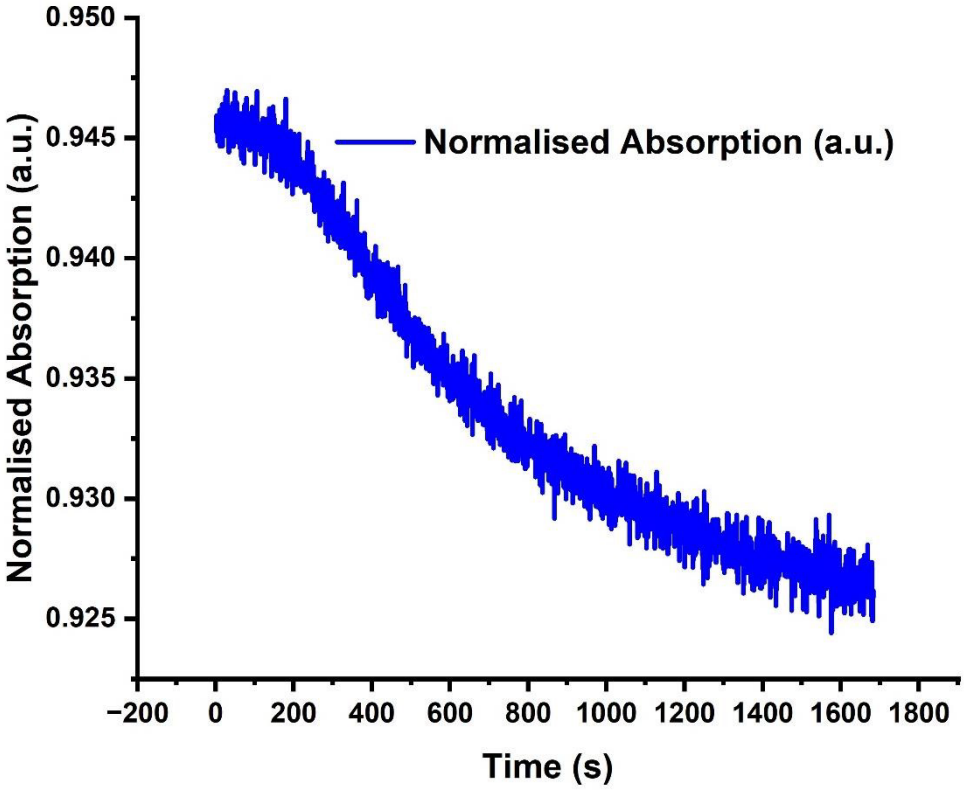

Supplementary Figure 8. Rh-K edge XANES trace as function of time under Ar at room temperature after reduction.

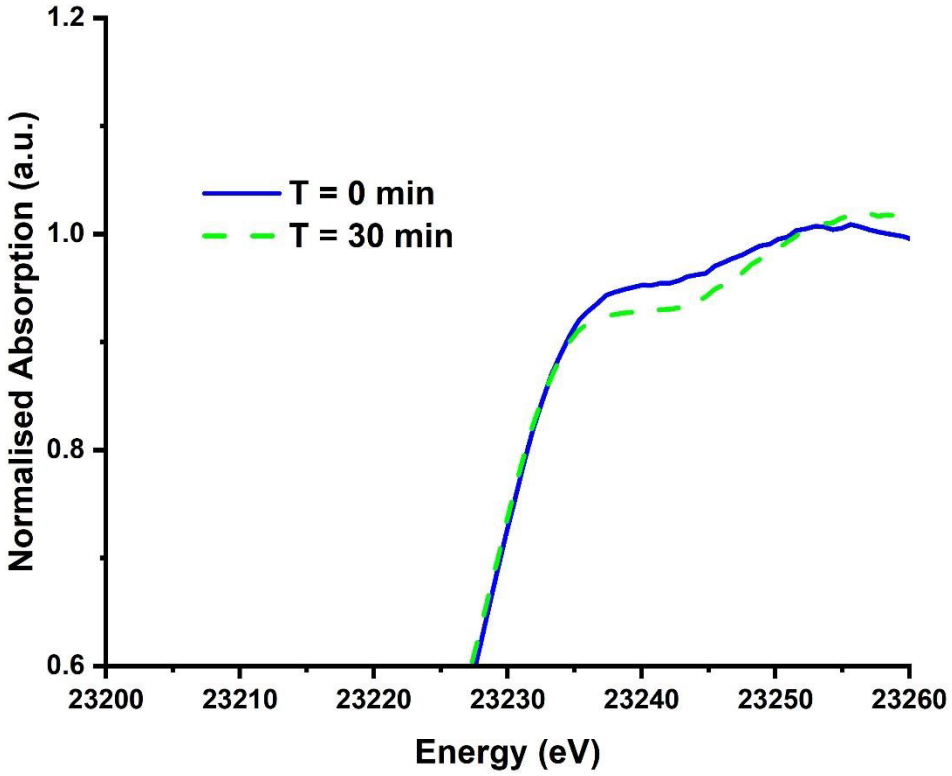

Supplementary Figure 9. Rh-K edge XANES spectra under Ar at 0 and 30 min after reduction.

`

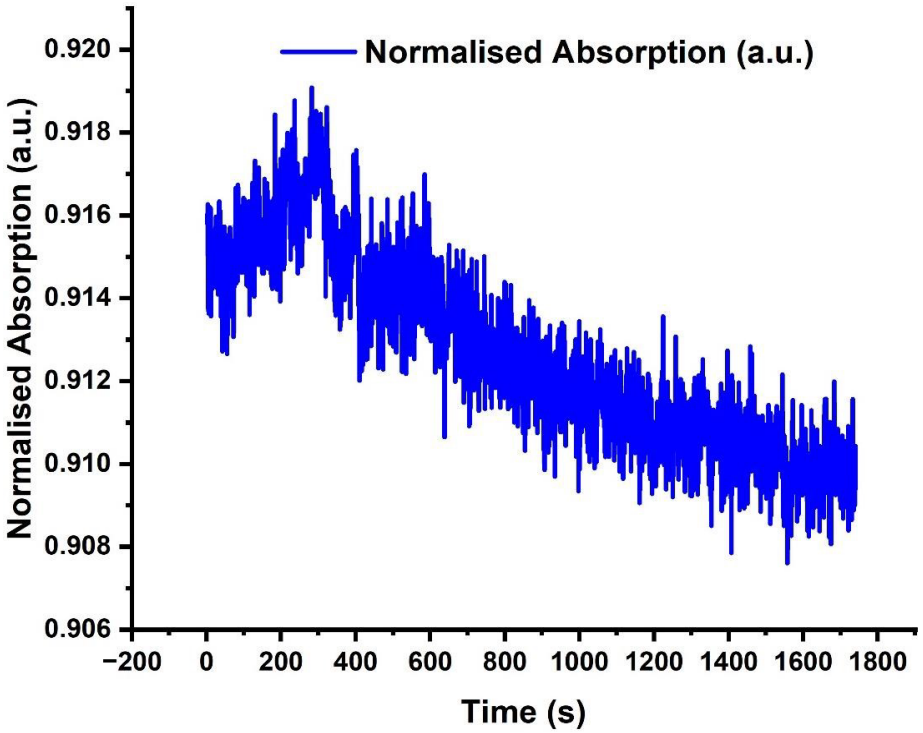

Supplementary Figure 10. Rh-K edge XANES trace as function of time under Ar at room temperature after flux reduction to 5.29%.

`

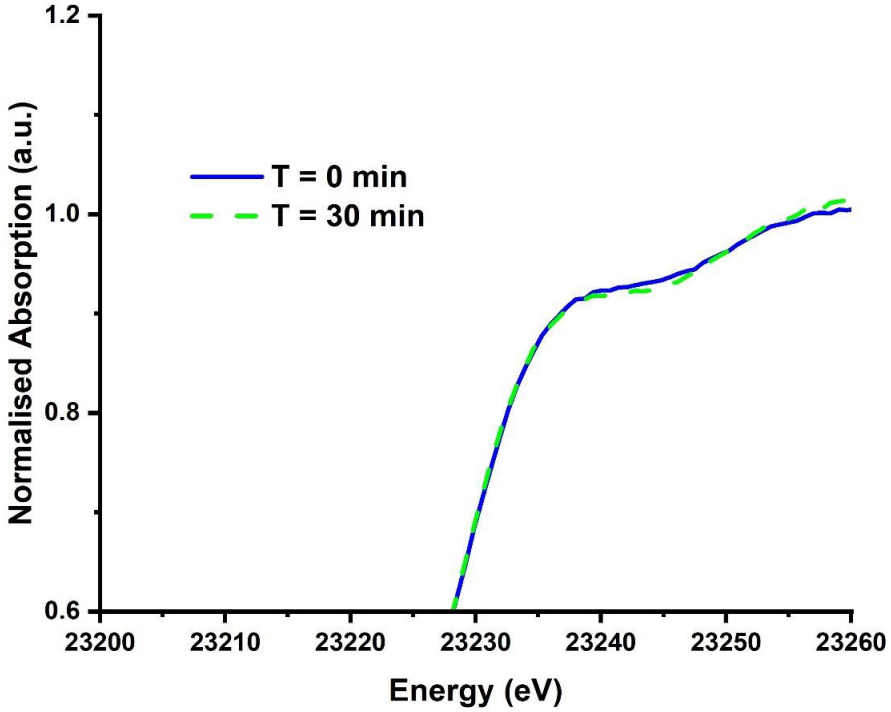

Supplementary Figure 11. Rh-K edge XANES spectra under Ar at 0 and 30 min after flux reduction to 5.29%.

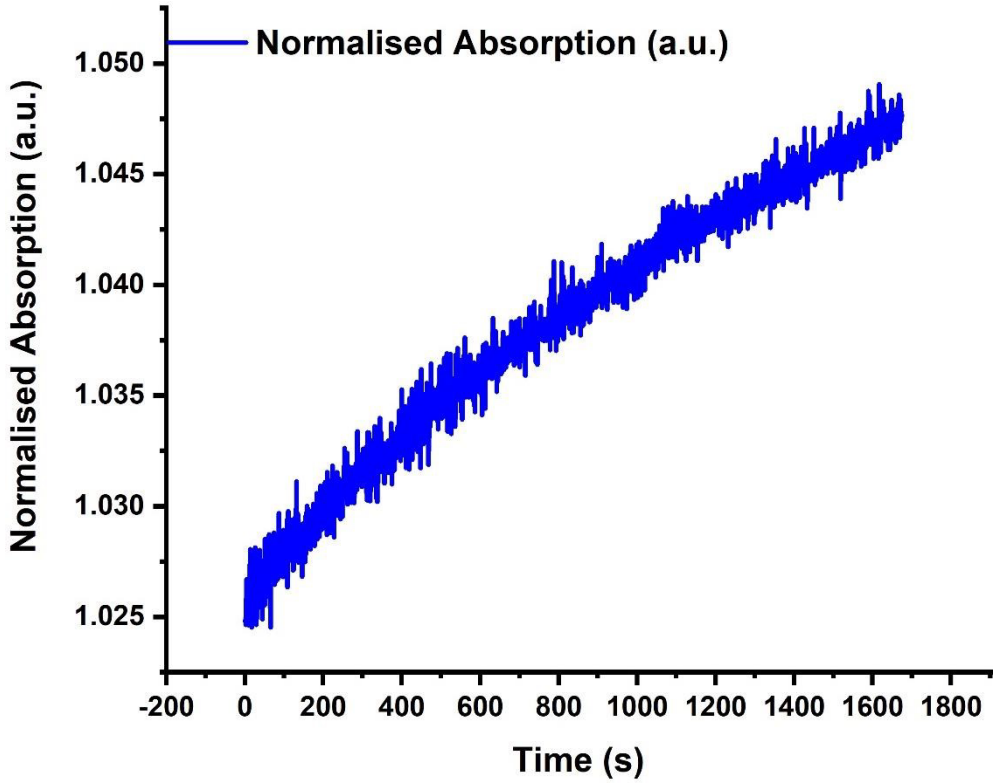

Supplementary Figure 12. Rh-K edge XANES trace as function of time under Ar at room temperature after radiative damage prevention on a fresh sample.

`

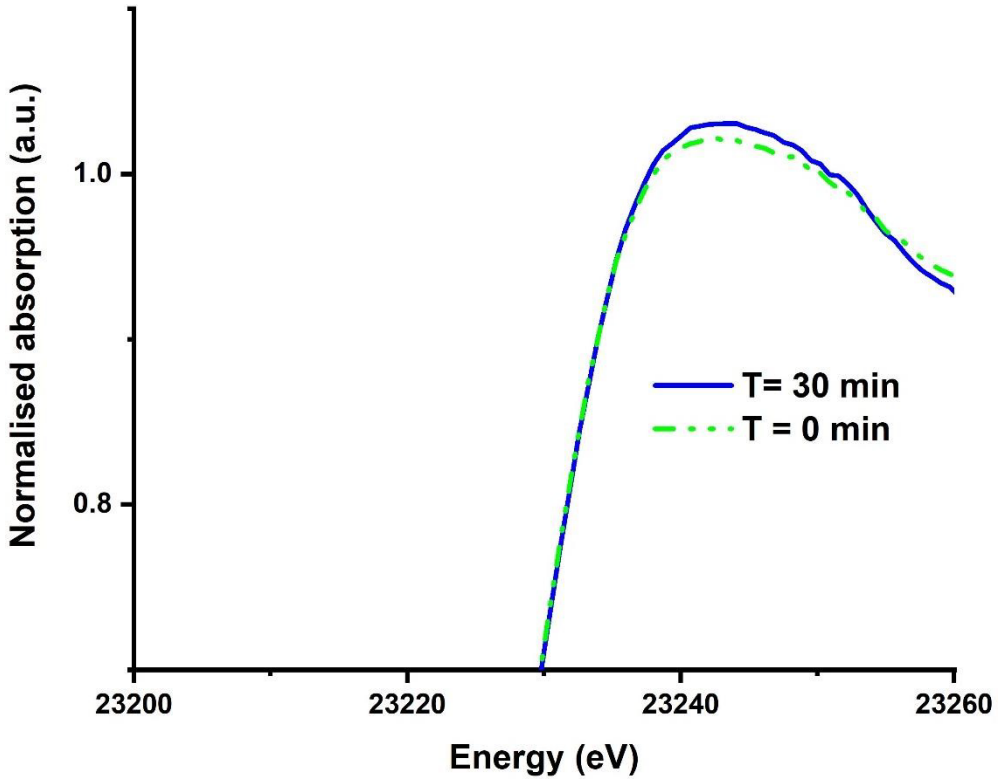

Supplementary Figure 13. Rh-K edge XANES spectra under Ar at 0 and 30 min after radiative damage prevention on a fresh sample

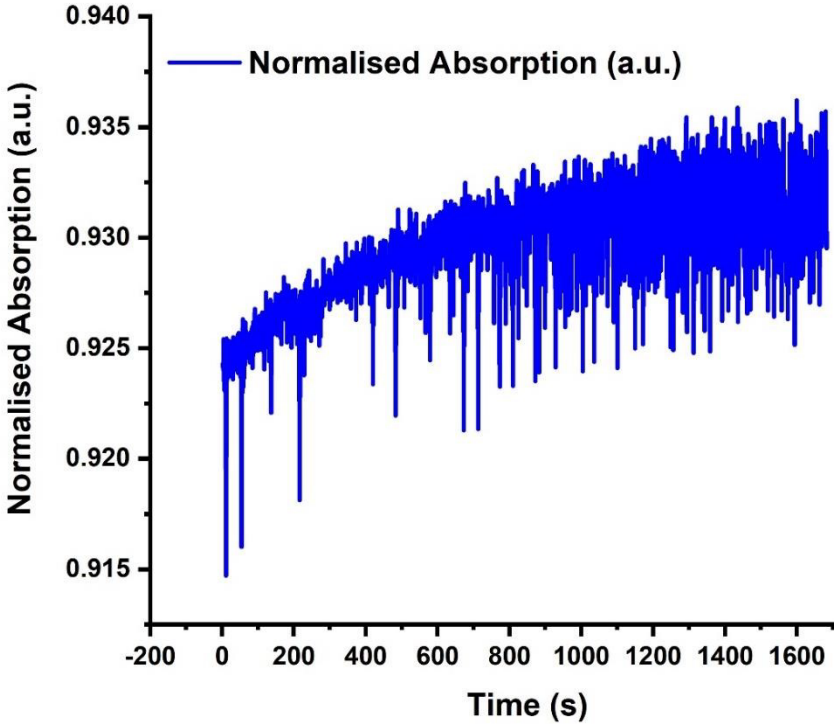

Supplementary Figure 14. Rh-K edge XANES trace as function of time during under Ar at room temperature after reduction.

`

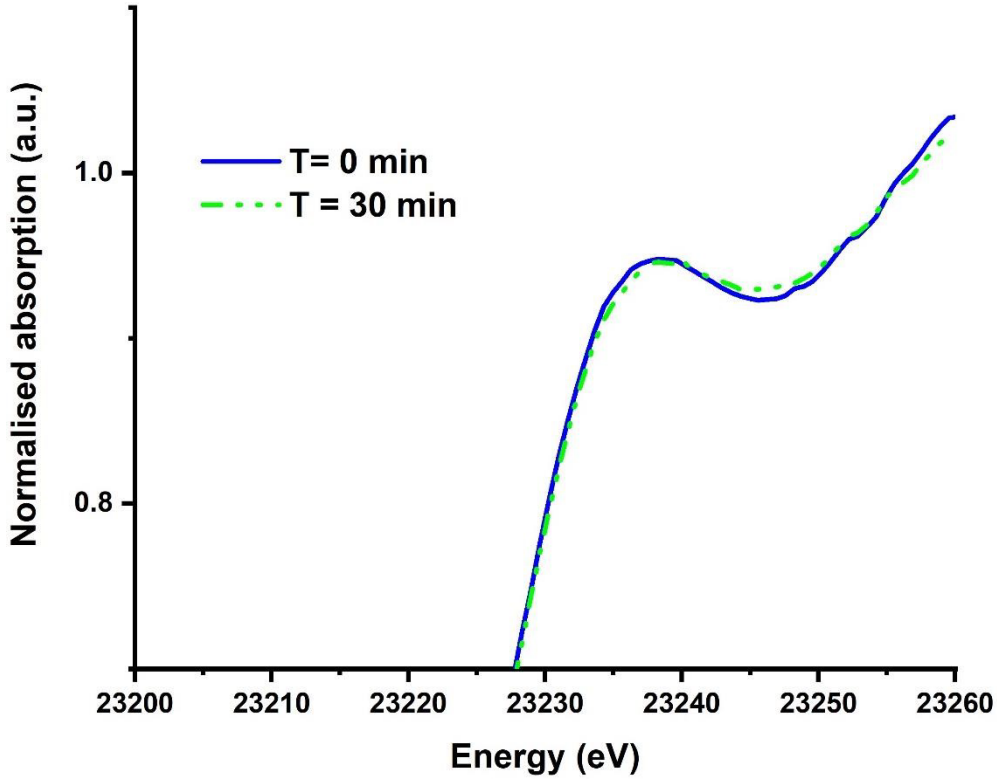

Supplementary Figure 15. Rh-K edge XANES spectra under Ar at 0 and 30 min on a fresh sample after reduction and flux reduction.

`

X-ray absorption spectroscopy results

The regeneration procedure employed in the experiment involves flowing H_2 at 180 °C and, after 15 minutes, the gas was switched to Ar for 5 min, followed by O_2 for 15 min, Ar for 15 min, H_2 for 15 min and then Ar until the sample was cooled down. In figure S8 are shown the spectra of the sample within the reactor, collected after different regeneration cycles, at different points. As shown from the XANES, no evident changes can be observed.

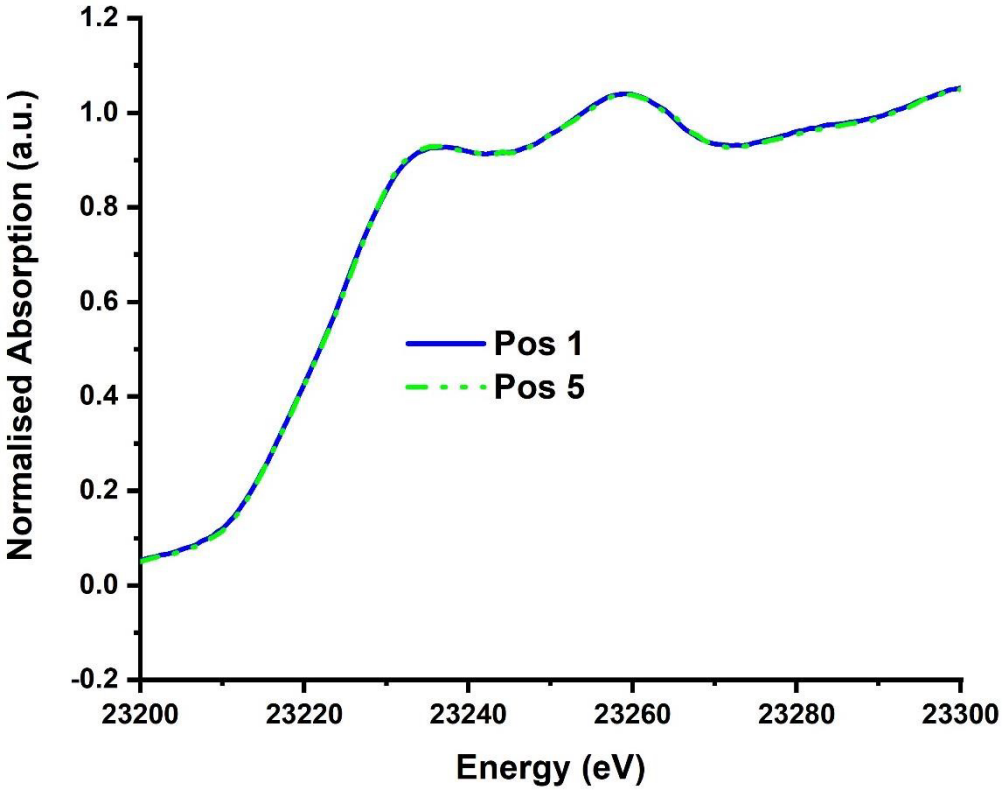

Supplementary Figure 16. XANES of different position after cleaning cycle

`

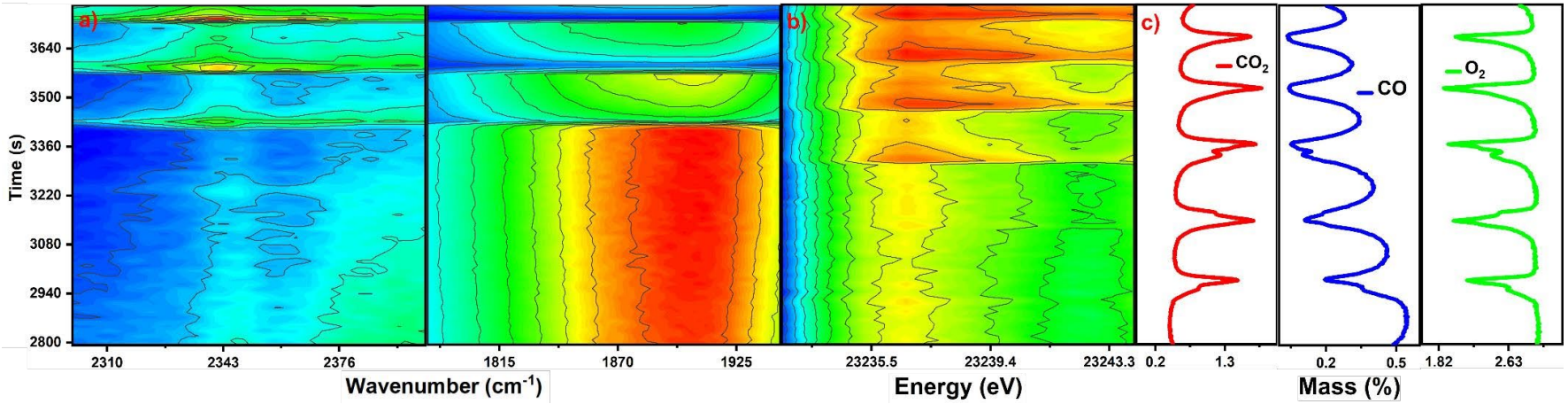

Supplementary Figure 17 From left to right: a) DRIFTS signature for CO (left) and CO_2 (right) evolution; b) XANES evolution; c) evolution of CO_2, CO, and O_2 concentration as function of time for the position 1.

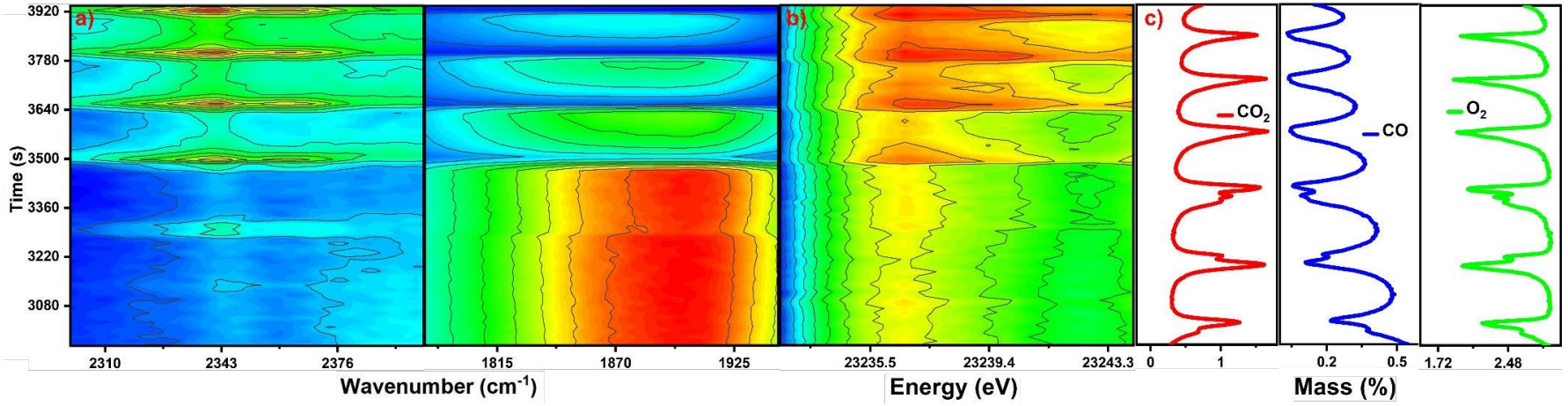

Supplementary Figure 18 From left to right: a) DRIFTS signature for CO (left) and CO_2 (right) evolution; b) XANES evolution; c) evolution of CO_2, CO, and O_2 concentration as function of time for the position 2.

`

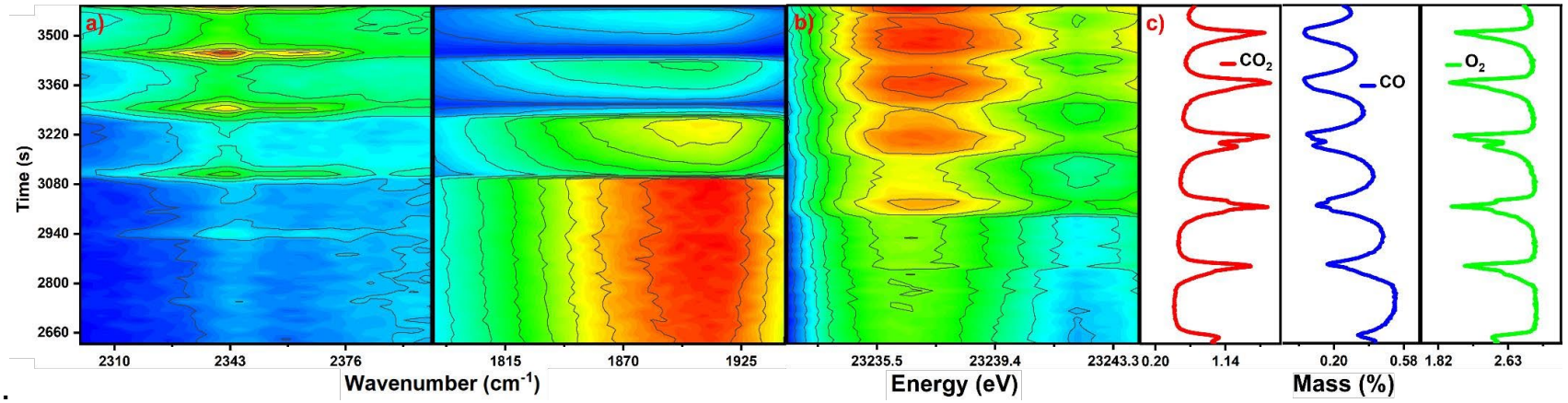

.

Supplementary Figure 19 From left to right: a) DRIFTS signature for CO (left) and CO_2 (right) evolution; b) XANES evolution; c) evolution of CO_2, CO, and O_2 concentration as function of time for the position 3.

`

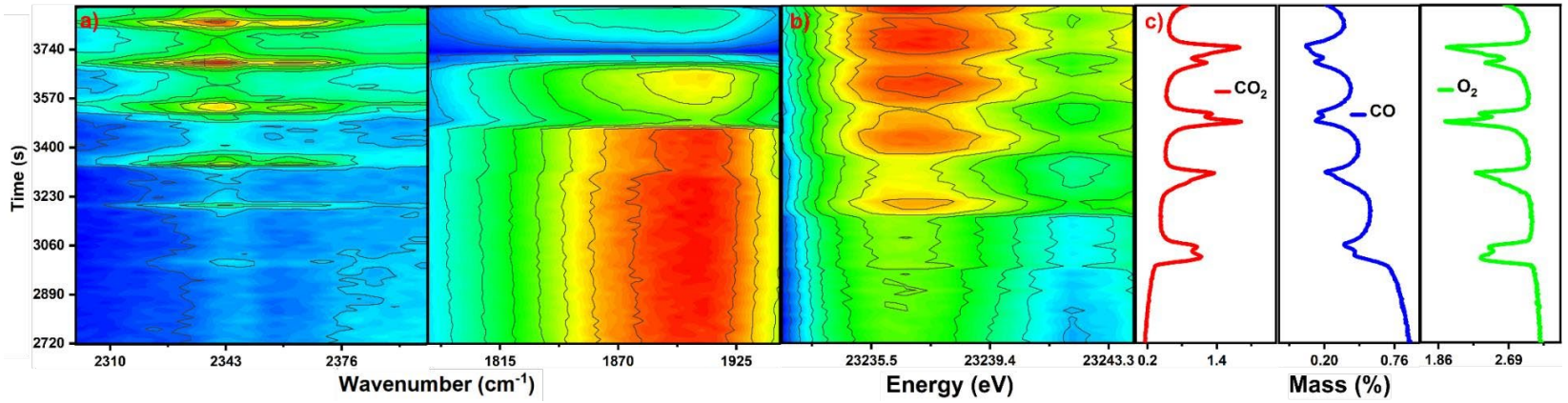

Supplementary Figure 20 From left to right: a) DRIFTS signature for CO (left) and CO_2 (right) evolution; b) XANES evolution; c) evolution of CO_2, CO, and O_2 concentration as function of time for the position 4.

`

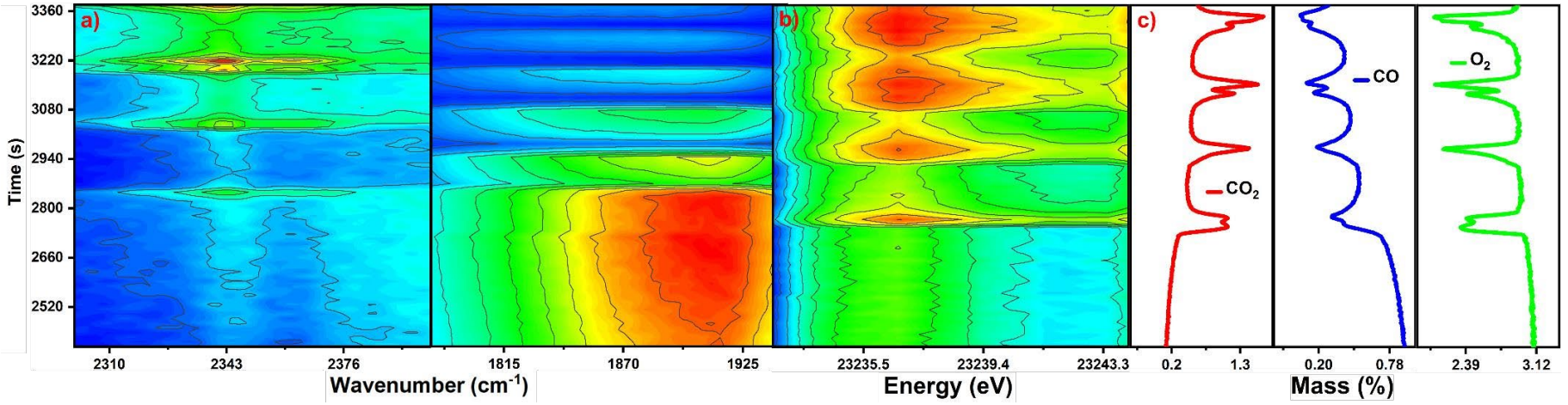

Supplementary Figure 21 From left to right: a) DRIFTS signature for CO (left) and CO_2 (right) evolution; b) XANES evolution; c) evolution of CO_2, CO, and O_2 concentration as function of time for the position 5.

`

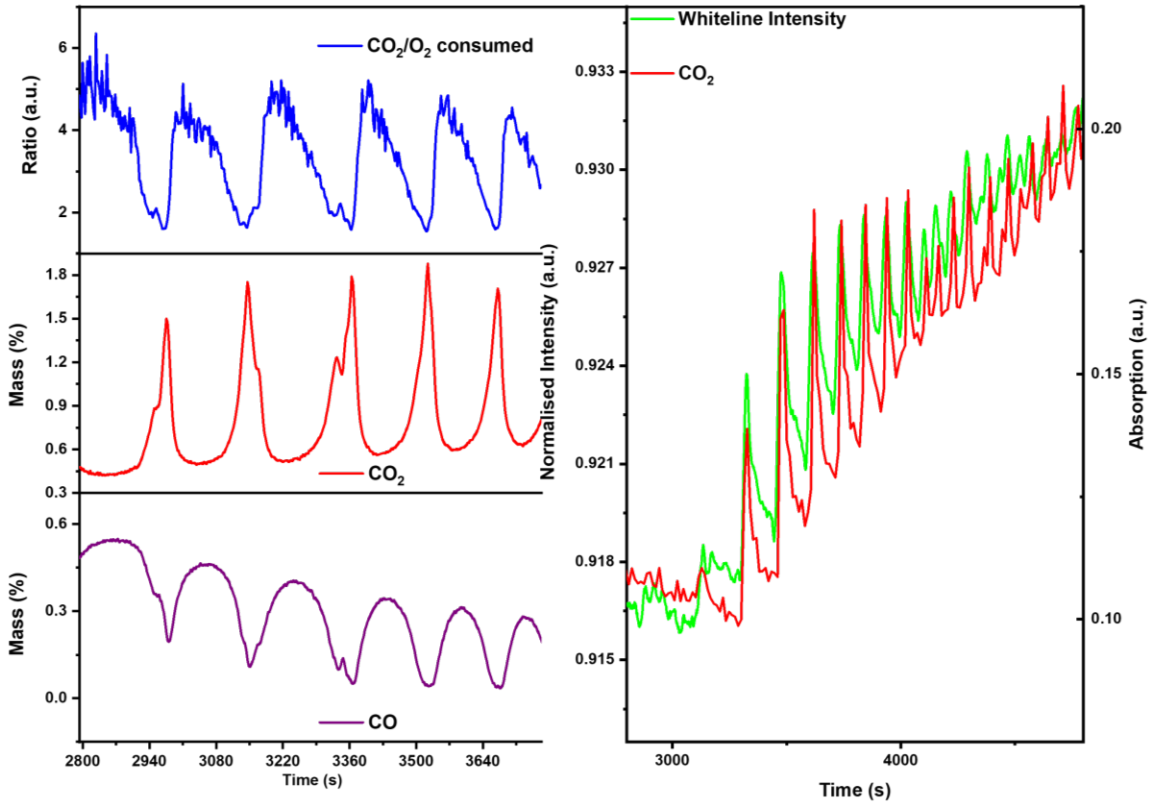

Supplementary Figure 22. a) CO_2 produced/O_2 consumed (top), CO_2 produced (middle), CO concentration (bottom); b) DRIFTS signal for CO_2(g) and XANES trace as function of time for the position 1 during temperature ramp.

`

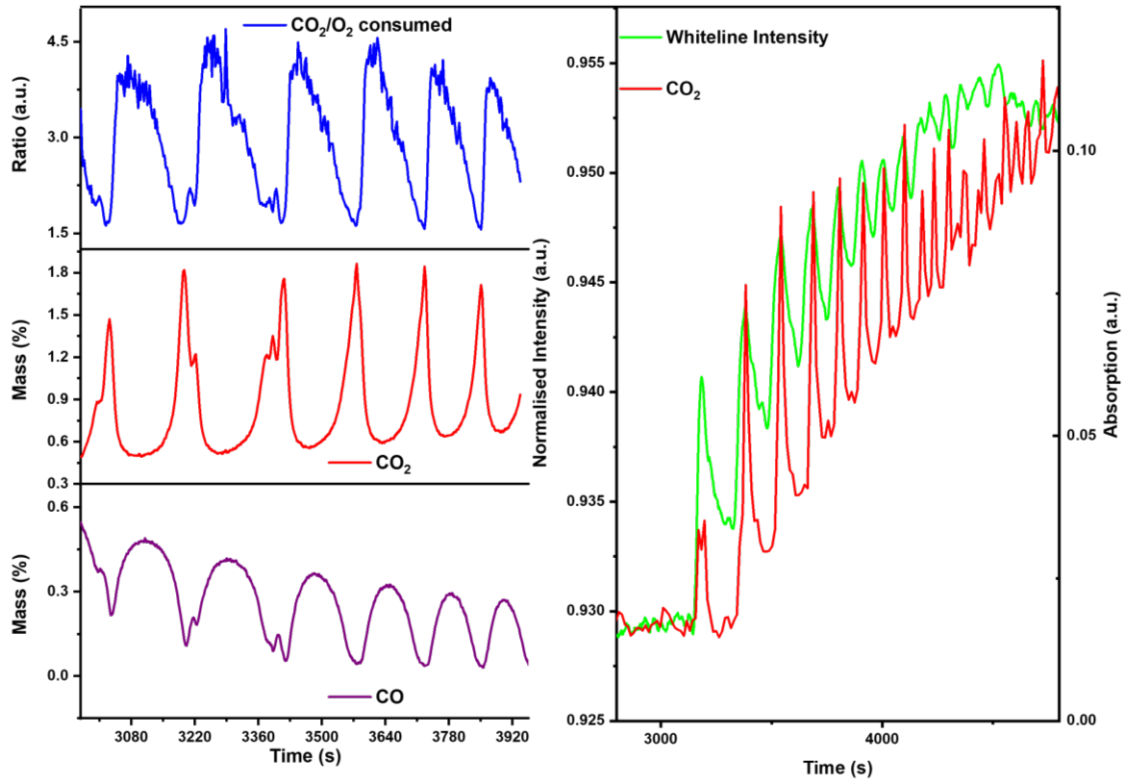

Supplementary Figure 23. a) CO_2 produced/O_2 consumed (top), CO_2 produced (middle), CO concentration (bottom); b) DRIFTS signal for CO_2(g) and XANES trace as function of

`

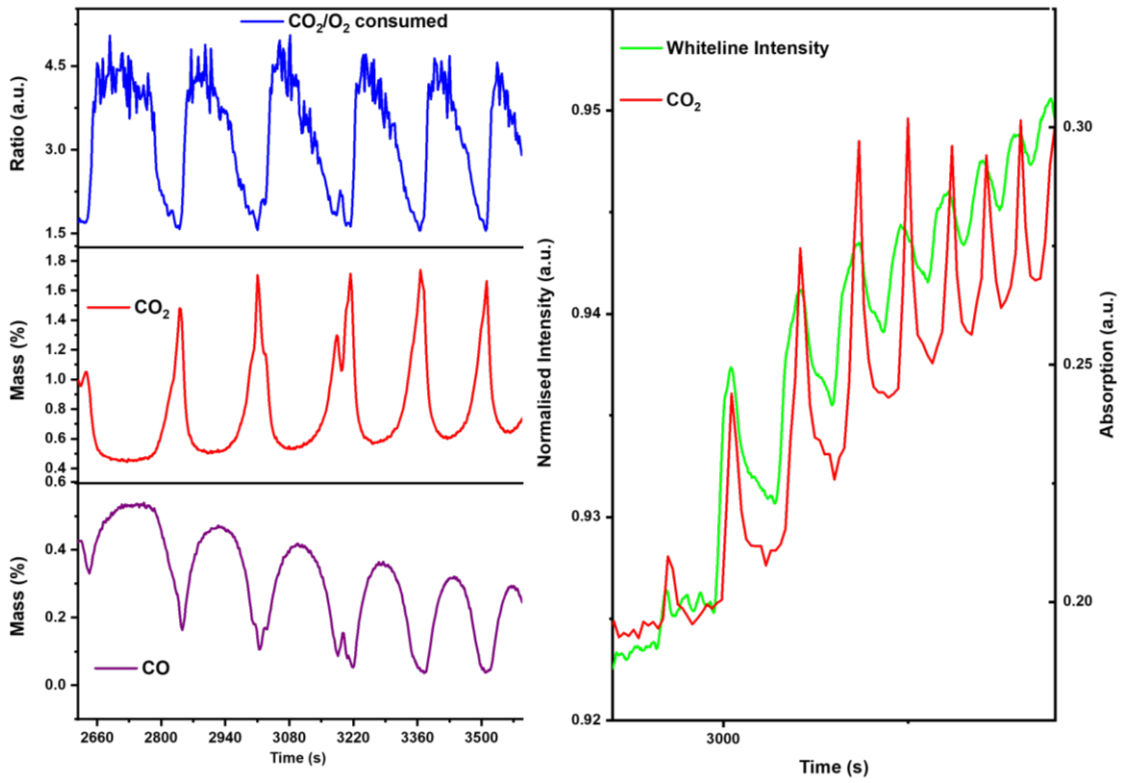

Supplementary Figure 24. a) CO_2 produced/O_2 consumed (top), CO_2 produced (middle), CO concentration (bottom); b) DRIFTS signal for CO_2(g) and XANES trace as function of time for the position 3 during temperature ramp.

`

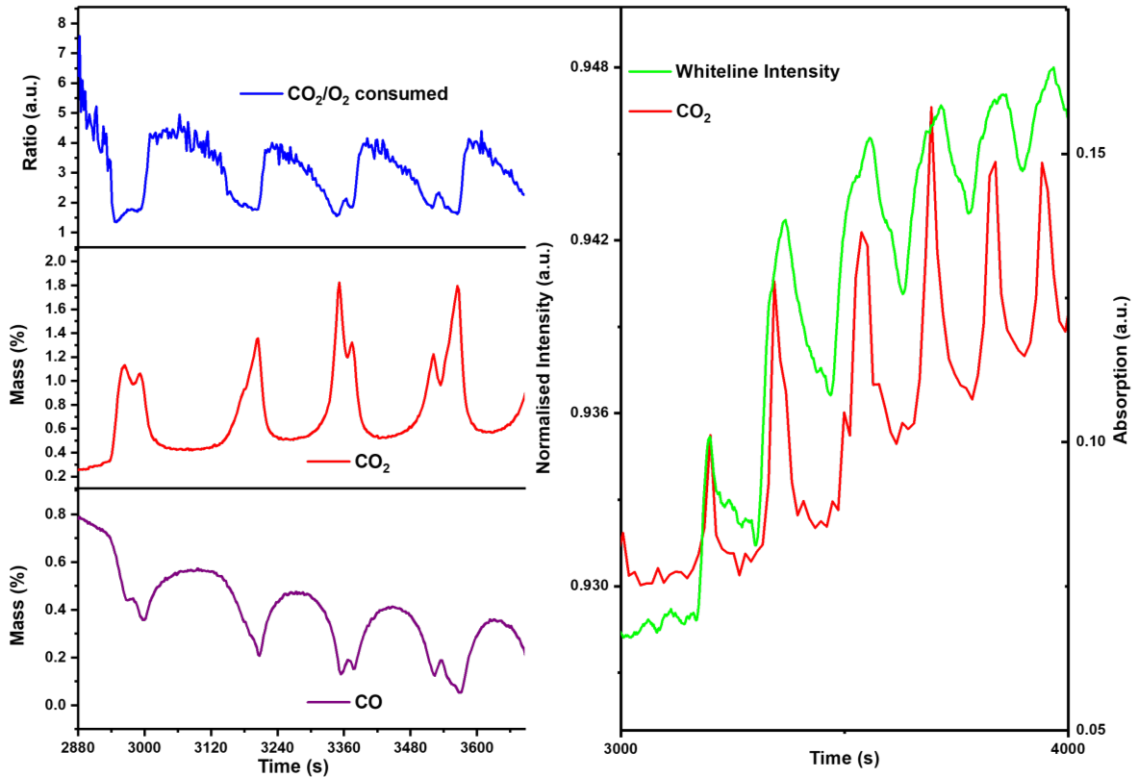

Supplementary Figure 25. a) CO_2 produced/O_2 consumed (top), CO_2 produced (middle), CO concentration (bottom); b) DRIFTS signal for CO_2(g) and XANES trace as function of

`

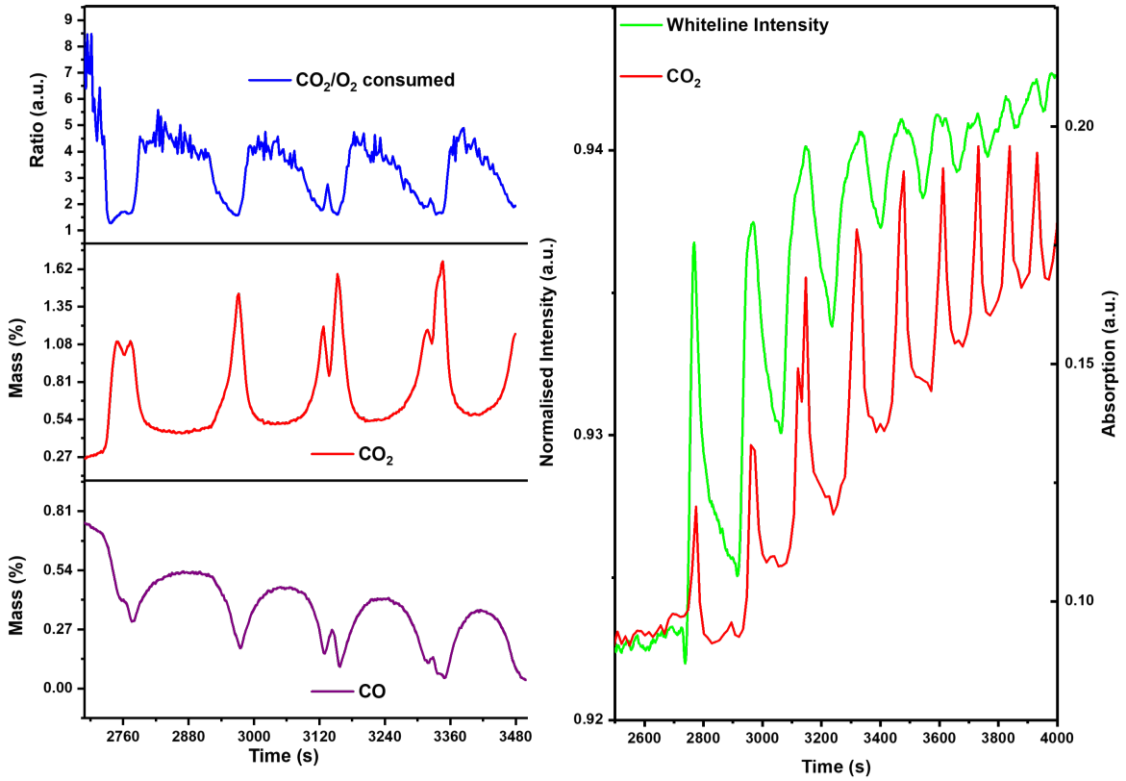

Supplementary Figure 26. a) CO_2 produced/O_2 consumed (top), CO_2 produced (middle), CO concentration (bottom); b) DRIFTS signal for CO_2(g) and XANES trace as function of time for the position 5 during temperature ramp.

IR data processing:

The data, collected in the range 4000 to 1000 cm^{-1} is first cropped to the region of interest, 2500-1500 cm^{-1}. The data is then imported on Origin software (Origin 2022b) and the background removal function is used to minimise the baseline changes which occur due to temperature change. Subsequently, the intensity of the IR peak at specific position (Rh^0 2060 (linear) and 1889 (bridging), $Rh^1(CO)_2$, 2092 (symmetrical) and 2020 (asymmetrical) cm^{-1}, Rh(CO) associated with Rh oxidation >1 at 2132 cm^{-1}, and gas phase CO2, 2340 cm^{-1}).

`

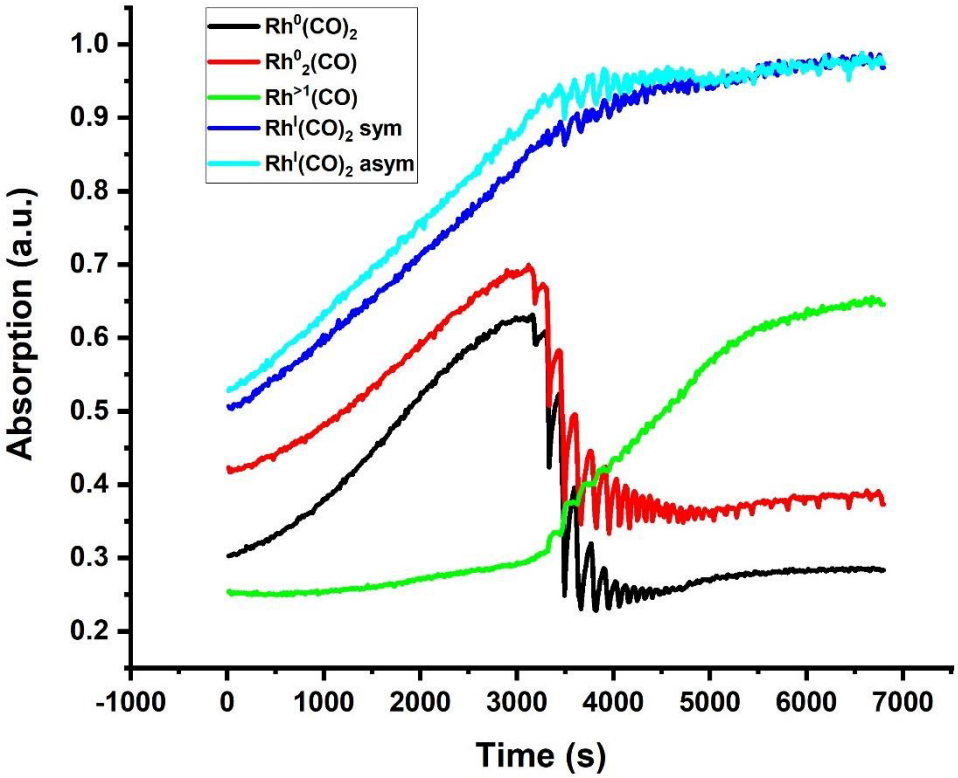

Supplementary Figure 27: DRIFTS signal for CO adsorbed on Rh at spatial position 6.

X-ray photoelectron spectroscopy (XPS) data

`

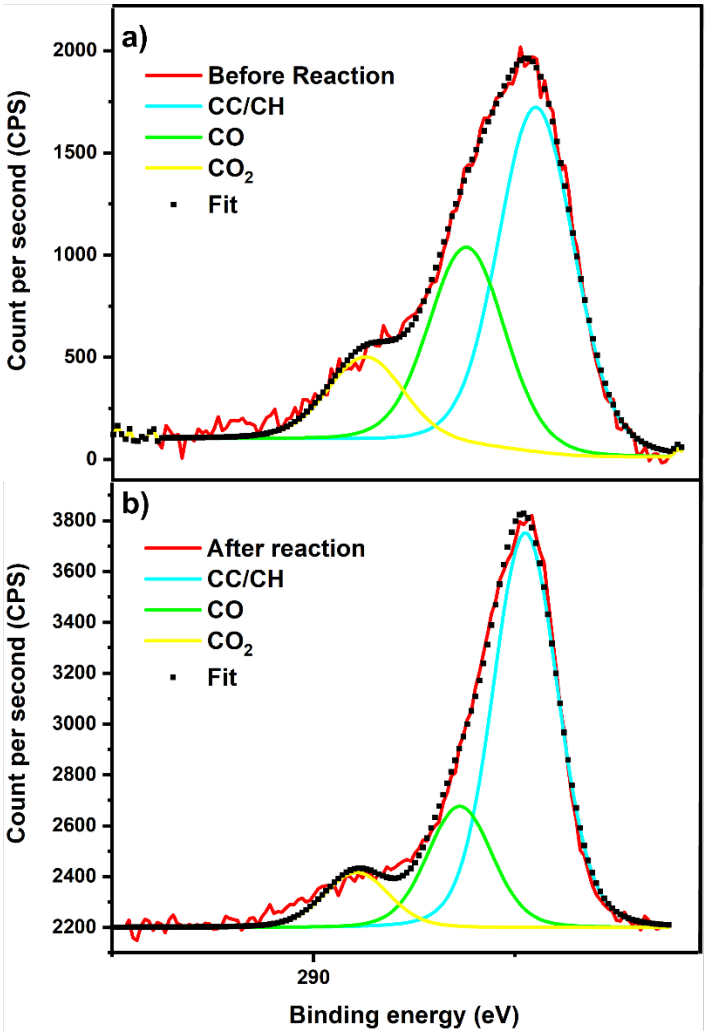

Supplementary Figure 28. XPS spectra at C energy of Rh/Al_2O_3 before and after reaction.

`

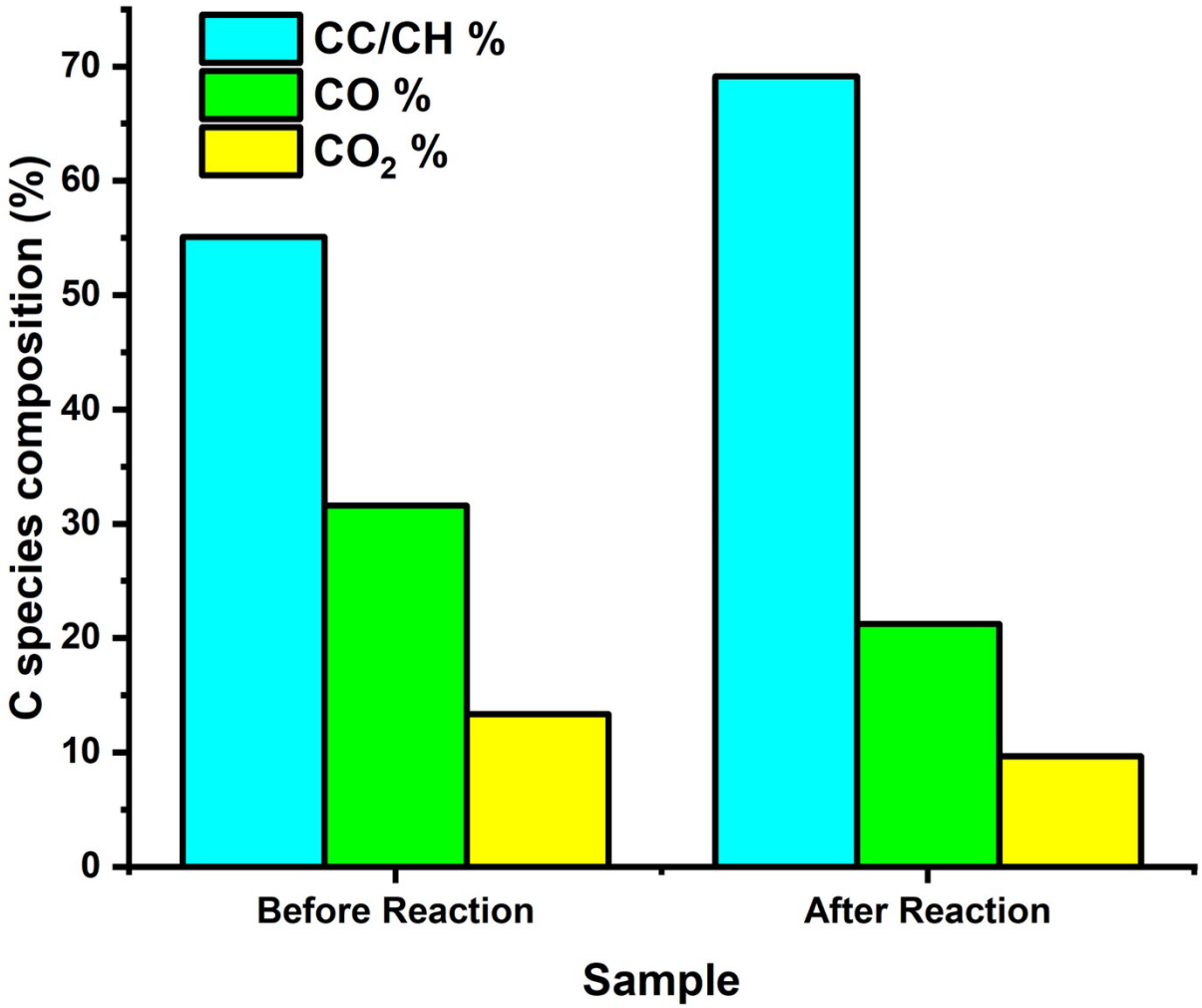

Supplementary Figure 29. Carbon speciation obtained through XPS of Rh/Al_2O_3 before and after reaction.

`

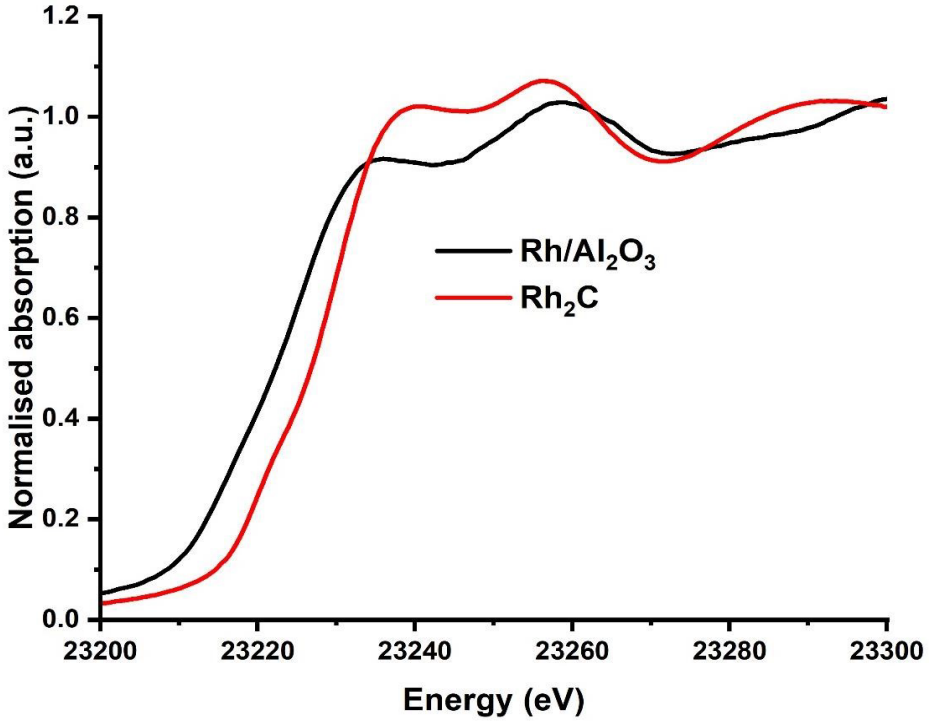

Supplementary Figure 30. Rh/Al_2O_3 during CO oxidation reaction and Rh_2C XANES data. The data shows a completely different structure in the sample

`

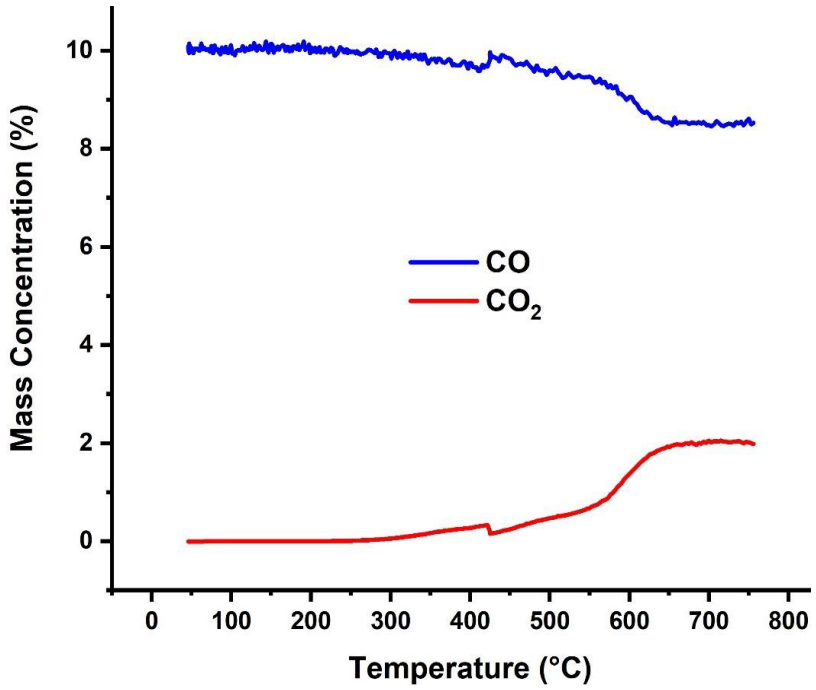

Supplementary Figure 31. Percentage mass concentration for CO and CO_2 (m/z 28 and 44 respectively) obtained through mass spectrometry during CO reaction on Rh/Al_2O_3 in absence of oxygen, as function of temperature.

Computational calculations

The computed $\boldsymbol{\sigma}$ for each surface are reported in Table S1. Consistent with previous studies,[1] our calculated surface energies confirm the {001} surfaces to be the most stable for all the systems investigated.

Supplementary Table 1. Calculated properties of the (001), (011) and (111) surfaces of Rh. Surface area ($\mathbf{a^2}$) is given in $Å^2$, whilst both unrelaxed ($\boldsymbol{\sigma_{unrel}}$) and relaxed ($\boldsymbol{\sigma_{rel}}$) surface energies are given in J/m^2.

PBE	$\mathbf{a^2}$	$\boldsymbol{\sigma_{unrel}}$	$\boldsymbol{\sigma_{rel}}$
(001)	57.4754	3.85	2.80
(011)	81.2825	3.57	3.23
(111)	99.5504	2.93	2.92
Scan			
(001)	57.4754	3.66	3.64
(011)	79.3530	3.76	3.70
(111)	97.1872	3.40	3.40

`

Carbon adsorption of carbon was calculated with reference to: bulk graphite, gas phase CO and carbon formed by the oxidation of CO to C + O_2 (see table 1). The values calculated are consistent throughout the two functional benchmarked with the obvious exception of the results with reference to graphite. This is explained by the higher formation energy of the elemental carbon seen using PBE.

Supplementary Table 2. Carbon adsorption. Values shown in eV with reference to: bulk graphite ($\Delta E_{Graphite}$), atomic carbon ($\Delta E_{C,surf}$) or CO – ½ O_2 (ΔE_{CO-O}).

Rh(001)	[a]$\Delta E_{Graphite}$	[a]$\Delta E_{C,Atom}$	[a]ΔE_{CO-O}	[b]$\Delta E_{Graphite}$	[b]$\Delta E_{C,Atom}$	[b]ΔE_{CO-O}
1C	-0.56	-8.60	0.00	-2.30	-8.31	0.00
2C	-0.36	-8.40	0.20	-2.11	-8.13	0.18
3C	-0.27	-8.31	0.29	-1.94	-7.95	0.36
4C	-0.09	-8.13	0.47	-1.69	-7.70	0.61
Rh(011)						
1C	2.04	-6.00	2.59	0.49	-5.53	2.78
2C	0.76	-7.28	1.32	0.49	-5.52	2.79
3C	0.79	-7.25	1.35	0.50	-5.51	2.80
4C	1.12	-6.92	1.67	0.51	-5.50	2.81
Rh(111)						
1C	0.45	-7.59	1.00	-1.24	-7.26	1.05
2C	0.65	-7.39	1.21	-1.21	-7.22	1.09
3C	0.77	-7.27	1.32	-1.15	-7.17	1.14
4C	0.75	-7.29	1.30	-1.03	-7.04	1.27

[a]PBE functional. [b]Scan functional.

Both functional also compute consistent carbon monoxide adsorption energies arose each surface studied with the exception of the values given in reference to the carbonated (011)surface. This is explained by the low adsorption energy of carbon on this surface as calculated by the PBE functional.

`

Supplementary Table 3. Carbon monoxide adsorption. Values shown in eV with reference to either gas phase CO ($\Delta E_{CO,mol}$) or the carbon loaded surface ($\Delta E_{C,surf}$).

Rh(001)	[a]$\Delta E_{CO,mol}$	[a]$\Delta E_{C,surf}$	[b]$\Delta E_{CO,mol}$	[b]$\Delta E_{C,surf}$
1CO	-2.36	-2.36	-2.50	-2.50
2CO	-2.35	-2.55	-2.46	-2.64
3CO	-2.29	-2.58	-2.39	-2.75
4CO	-2.28	-2.75	-2.41	-3.02
Rh(011)				
1CO	-2.28	-3.60	-2.37	-5.16
2CO	-2.29	-3.61	-2.38	-5.17
3CO	-2.28	-3.63	-2.37	-5.16
4CO	-2.27	-3.94	-2.36	-5.17
Rh(111)				
1CO	-2.22	-3.22	-2.24	-3.30
2CO	-2.17	-3.38	-2.26	-3.35
3CO	-2.13	-3.46	-2.25	-3.39
4CO	-2.14	-3.44	-2.22	-3.49

[a]PBE functional. [b]Scan functional.

Owing to the consistent performance of both functionals with regards to their predicted adsorption values, it was decided to calculate the reaction mechanisms of each facet with the PBE functional only. Supplementary equation 1−3 show the calculated reaction mechanisms depicted in figures 5 (see manuscript), respectively.

$$C + O_2 \rightarrow CO + O \qquad \text{(Supplementary equation 1)}$$

$$2CO \rightarrow CO_2 + C \qquad \text{(Supplementary equation 2)}$$

$$CO + O_2 \rightarrow CO_2 + O \qquad \text{(Supplementary equation 3)}$$

`

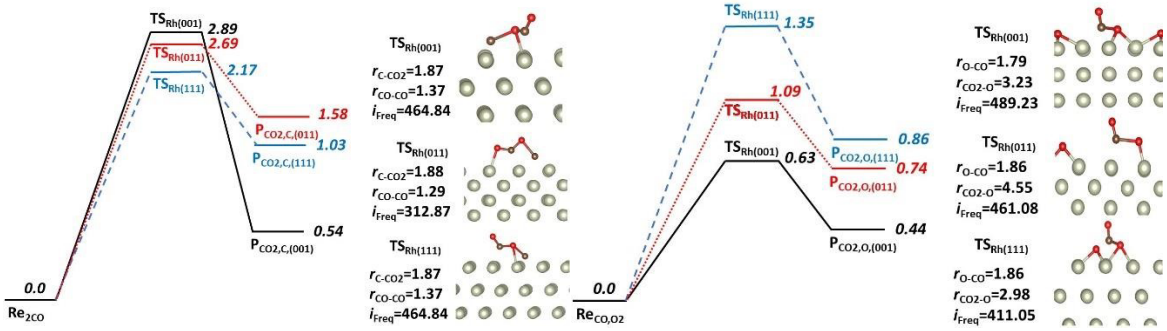

Supplementary Figure 32. Reaction landscape surface mediated: (left) Boudouard reaction, (right) carbon oxidation. Reaction landscapes for: (black solid line) Rh(001) surface, (red dotted line) Rh(011) surface and (blue dashed line) Rh(111) surface. All energies are given in eV with important transition state bond distances shown in Å. The negative frequency corresponding to the reaction coordinate for each transition state is given in cm^{-1}.

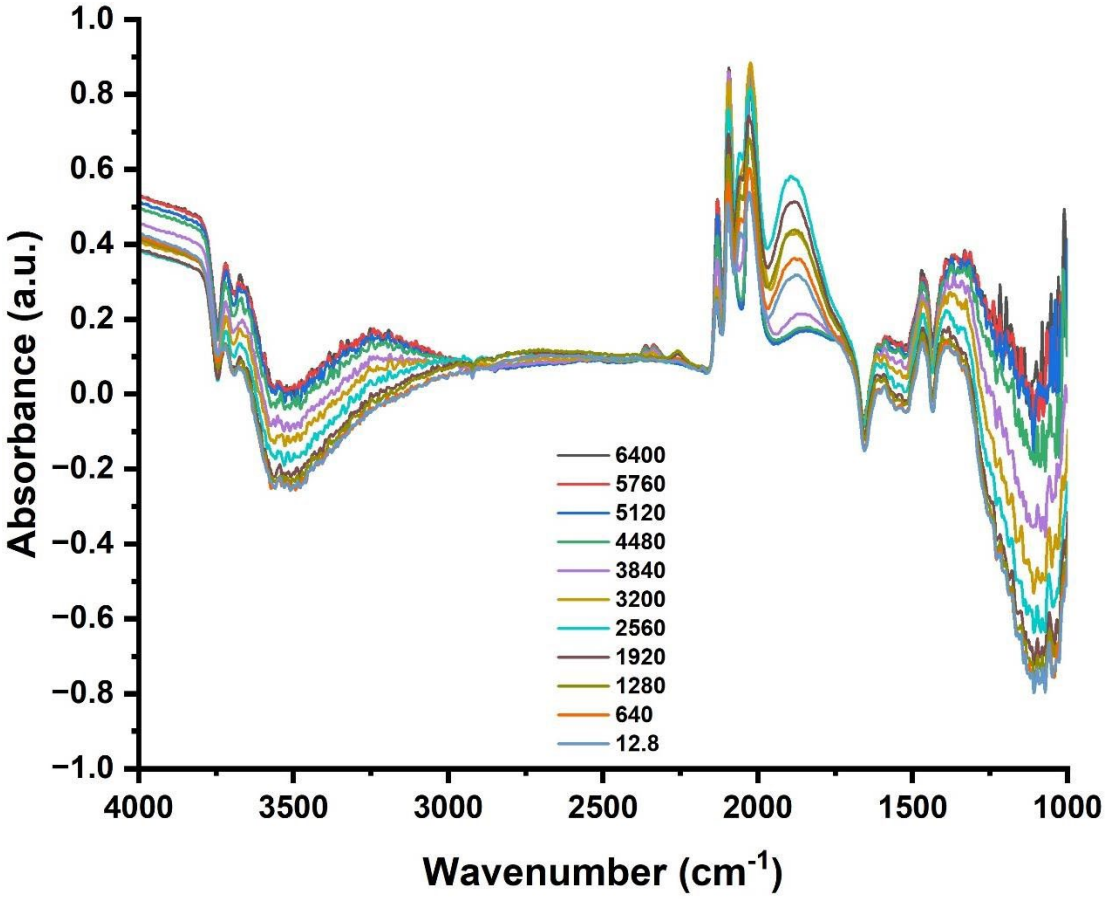

Supplementary Figure 33. IR spectrum between 4000 and 1000 cm^{-1} at different time position for at the catalyst bed outlet during temperature ramp (axial position 6).

`

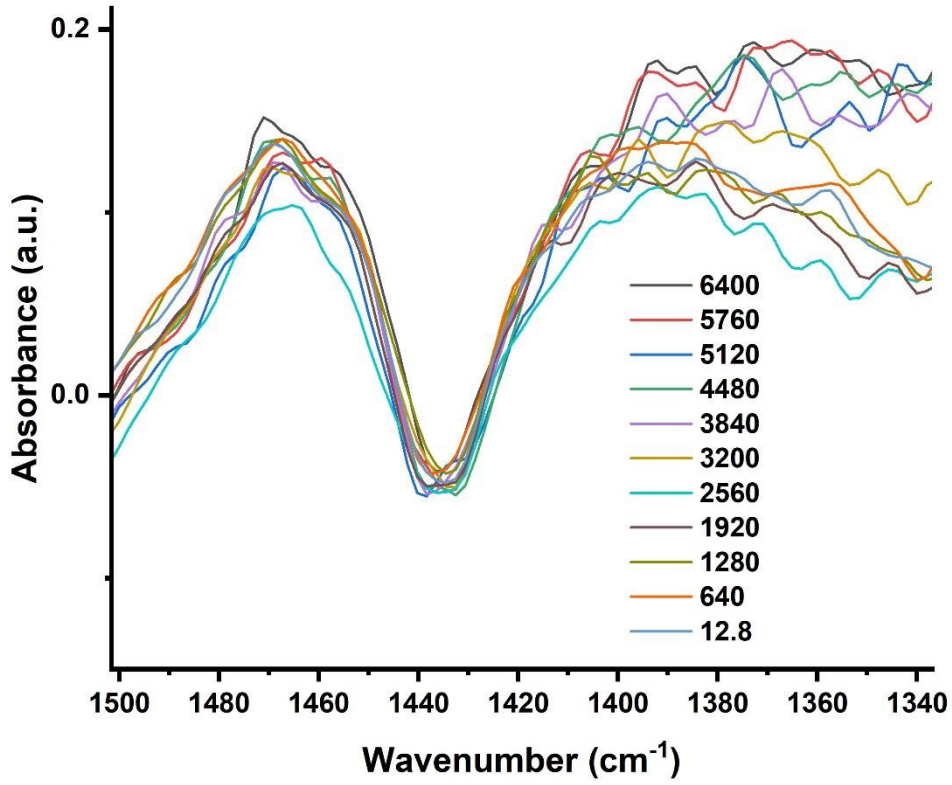

Supplementary Figure 34. IR spectrum of the region between 1500 and 1340 cm^{-1} showing the negative peak attributed to carbonates.

`

EXAFS analysis

Table S4 shows the extracted EXAFS fitting parameters, notably the primary Rh-Rh coordination numbers, at different axial positions. Within the associated error, we are unable to identify any systematic changes in Rh-Rh coordination number, and by extension, particle size as a function of the axial position. To reduce the associated error in the coordination number, both the amplitude reduction factor and mean-squared disorder parameter have been used as a fixed input parameter.

The spectra were analysed using Athena and Artemis from the Demeter IFEFFIT package[2,3]. The FEFF6 code was used to construct theoretical EXAFS signals that included singlescattering contributions from atomic shells through the nearest neighbours, using Rh as scatterer. The fit was performed using a k-range between 3 and 11.5 $Å^{-1}$ and an R range between 2.2 and 3 Å. The amplitude reduction factor (S_0^2) was fixed at 0.69, and the thermal disorder factor (σ^2) was fixed at 0.003 as obtained from fitting the bulk Rh foil reference.

Supplementary Table 4. EXAFS Fit results for Rh/Al_2O_3 at room temperature upon CO/O_2 breakthrough as a function of axial position

Axial Position	CN_{Rh-Rh}	R_{Rh-Rh} (Å)	ΔE	R_{factor}
1	7 ± 0.4	2.681 ± 0.006	-2 ± 1	0.007
2	7 ± 0.6	2.689 ± 0.008	-1 ± 2	0.02
3	6.2 ± 0.7	2.68 ± 0.01	-2 ± 2	0.03
4	7.7 ± 1	2.68 ± 0.01	-3 ± 3	0.03
5	6.7 ± 1	2.68 ± 0.01	1 ± 3	0.04
6	6.7 ± 1	2.68 ± 0.01	-4 ± 3	0.04

Fitting parameters: $S_0^2 = 0.69$ and $\sigma^2 = 0.003$ as determined by the use of a Rh foil standard; Fit range $3 < k < 11.5$ $Å^{-1}$, $2.2 < R < 3$ Å; number of independent points = 4.1.

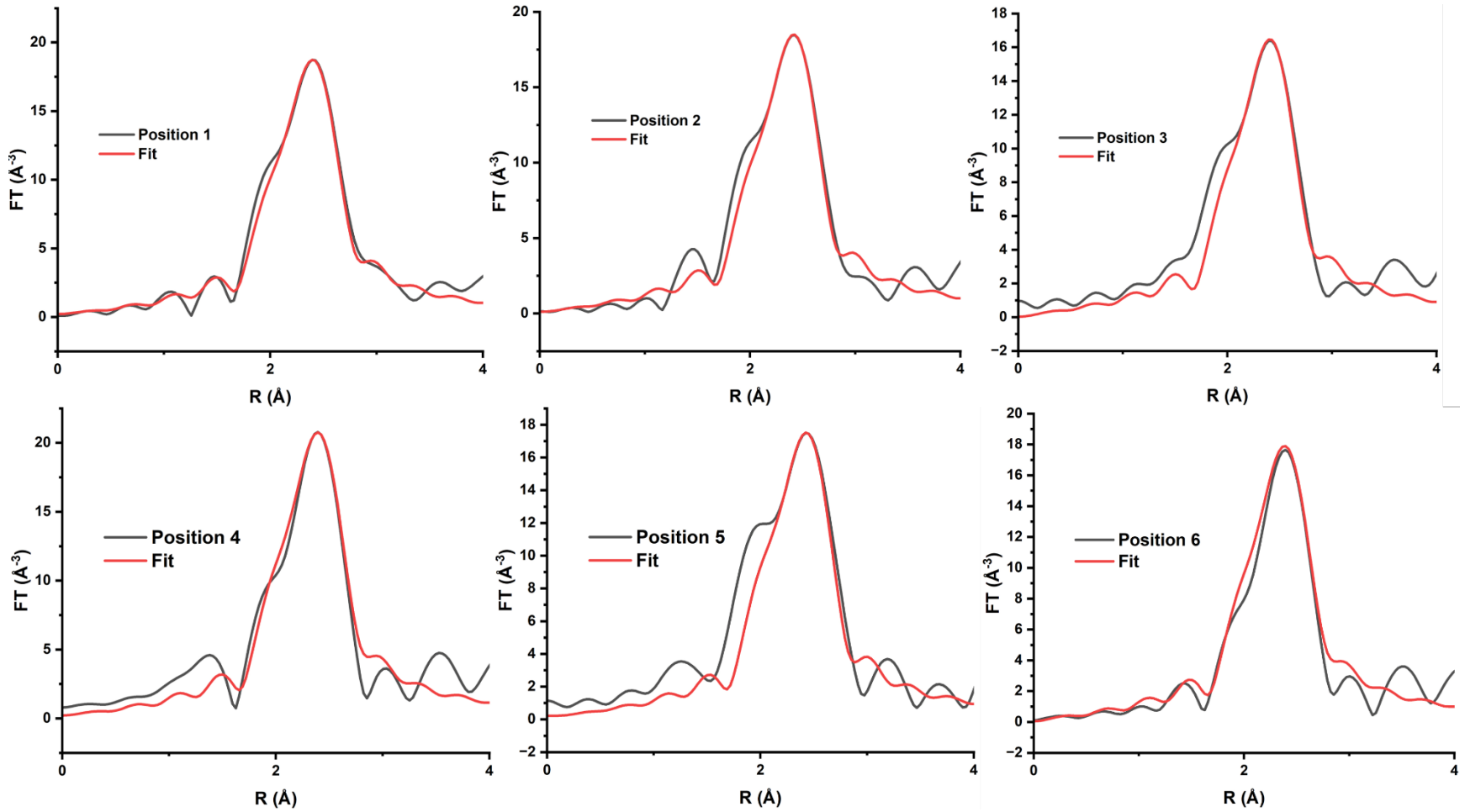

Supplementary Figure 35 Fourier Transform of EXAFS of Rh/Al_2O_3 at various position across the bed under CO/O_2 at T=0s

`

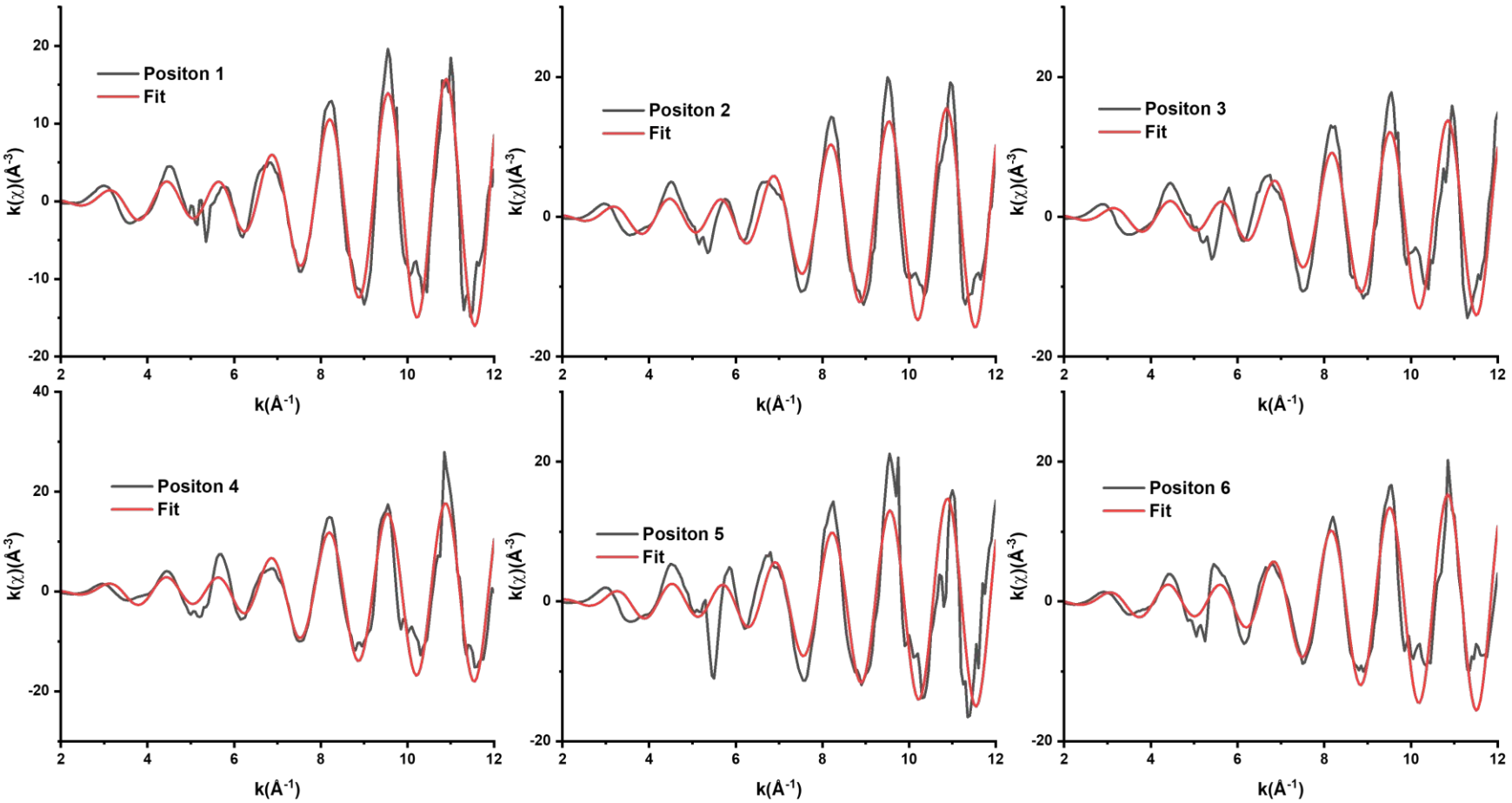

Supplementary Figure 36. k^3-weighted EXAFS fit of Rh/Al_2O_3 at various position across the bed under CO/O_2 at T=0s

`

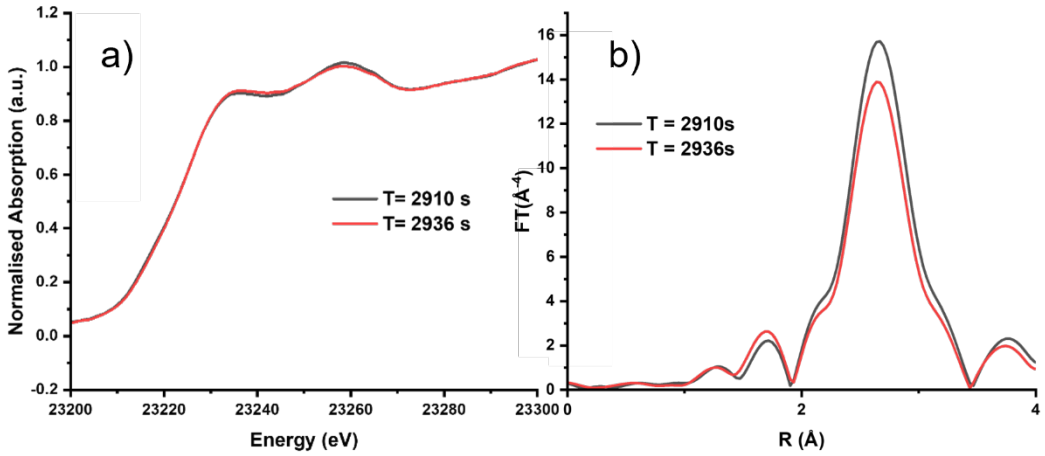

Supplementary Figure 37. a) XANES data; b) Fourier Transform of EXAFS. The time refer to the catalyst before the first burst of CO_2 and at the peak of the burst. Refer to figure 3b for an accurate comparison of timing.

Supplementary Table 5 EXAFS Fit results for Rh/Al_2O_3 for position 6 before and the peak of an oscillatory phenomena. Refer to figure 3b for an accurate comparison of timing

Time (s)	CN_{Rh-Rh}	R_{Rh-Rh} (Å)	σ_{Rh-Rh}	ΔE	R_{factor}
2910	6.5 ± 0.75	2.68 ± 0.005	0.005 ± 0.003	-4.3 ± 0.8	0.016
2936	6.3 ± 0.99	2.676 ± 0.007	0.0054 ± 0.001	-4.79 ± 1.2	0.0299

Fitting parameters: $S_0^2 = 0.69$ and $\sigma^2 = 0.003$ as determined by the use of a Rh foil standard; Fit range $3 < k < 11.5$ Å^{-1}, $2.2 < R < 3$ Å; number of independent points = 4.1.

MCR Analysis

The multivariate curve resolution (MCR) analysis was performed using pyMCR, employing constraints for unity concentration sum and non-negativity in spectral components and concentrations[4]. The MCR refinements were completed until convergence with percentage lack of fit as the loss function. Initialization of the spectral components was performed using the SIMPLISMA algorithm[5].

`

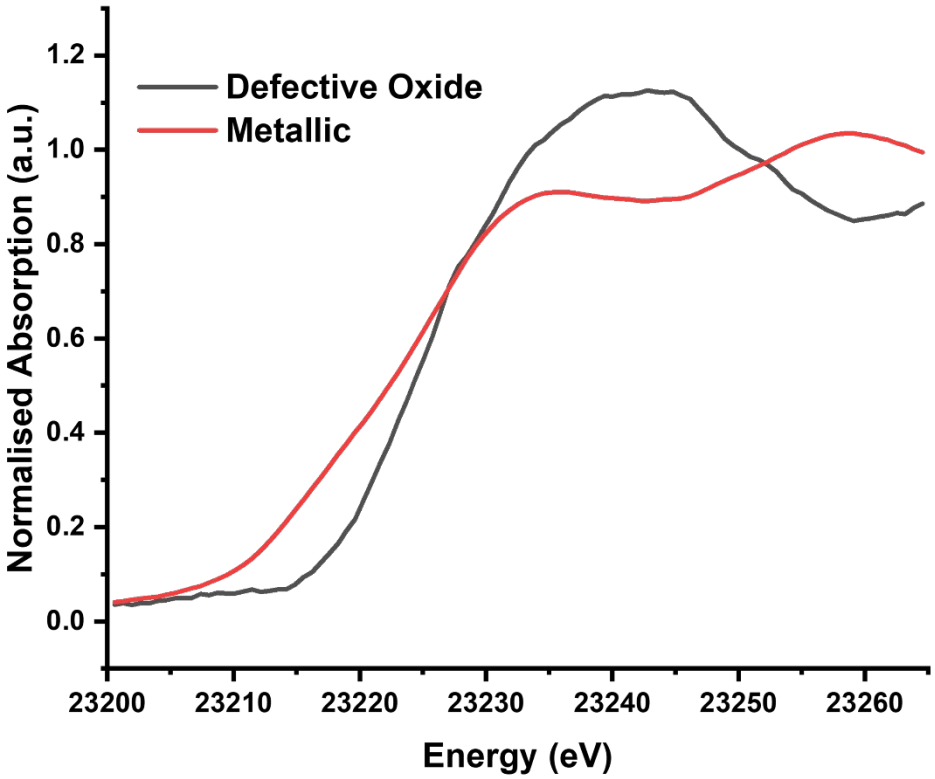

Supplementary Figure 38. Spectral component obtained from MCR analysis of the system indicating a defective Rh oxide and a metallic Rh phase.

`

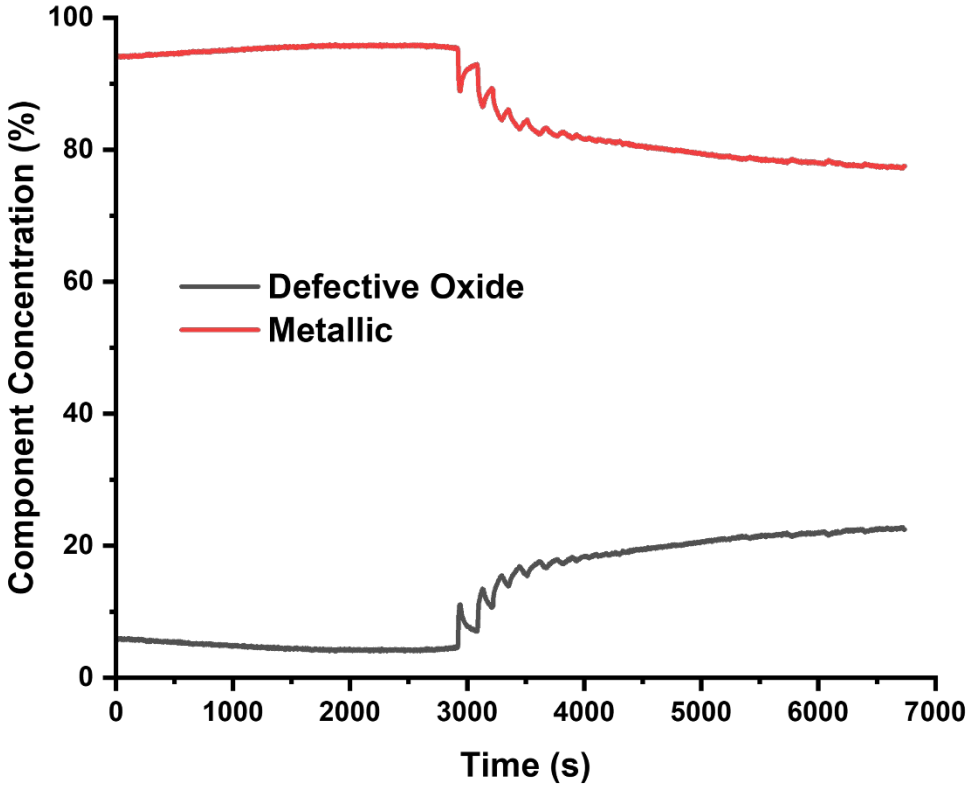

Supplementary Figure 39. Component concentrations as a function of time obtained from MCR analysis using the component in fig S37.

`

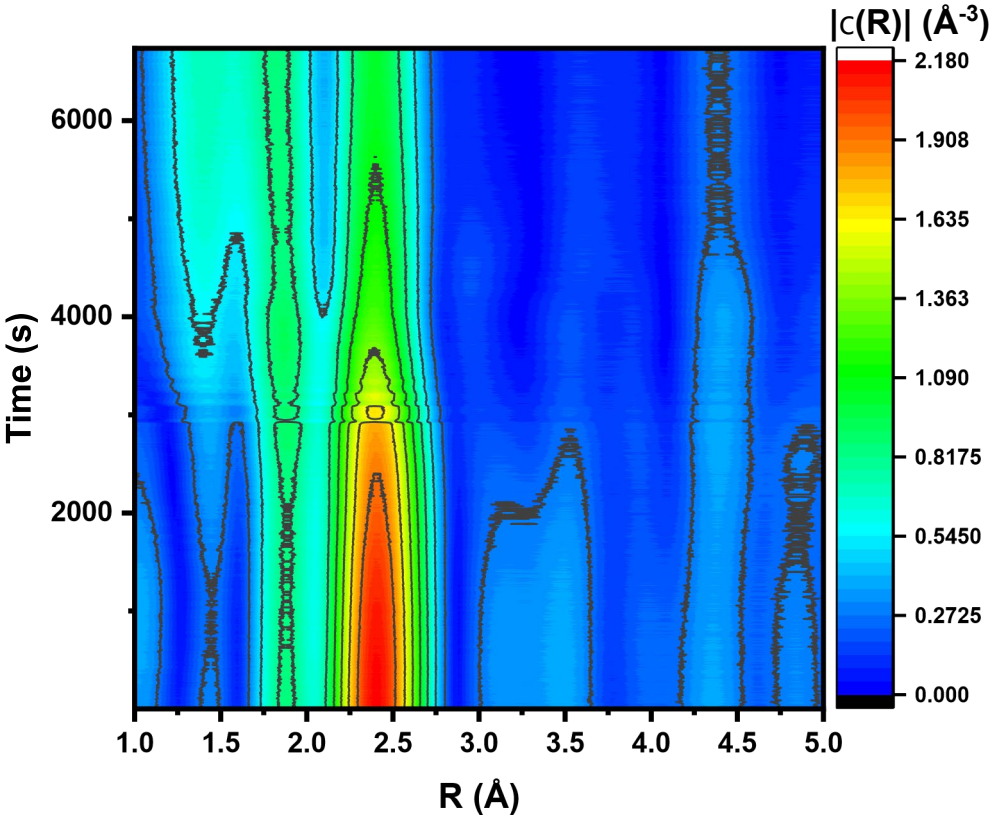

Supplementary Figure 40. Contour plot of XAFS Fourier Transform for Rh/Al_2O_3 as function of time.

`

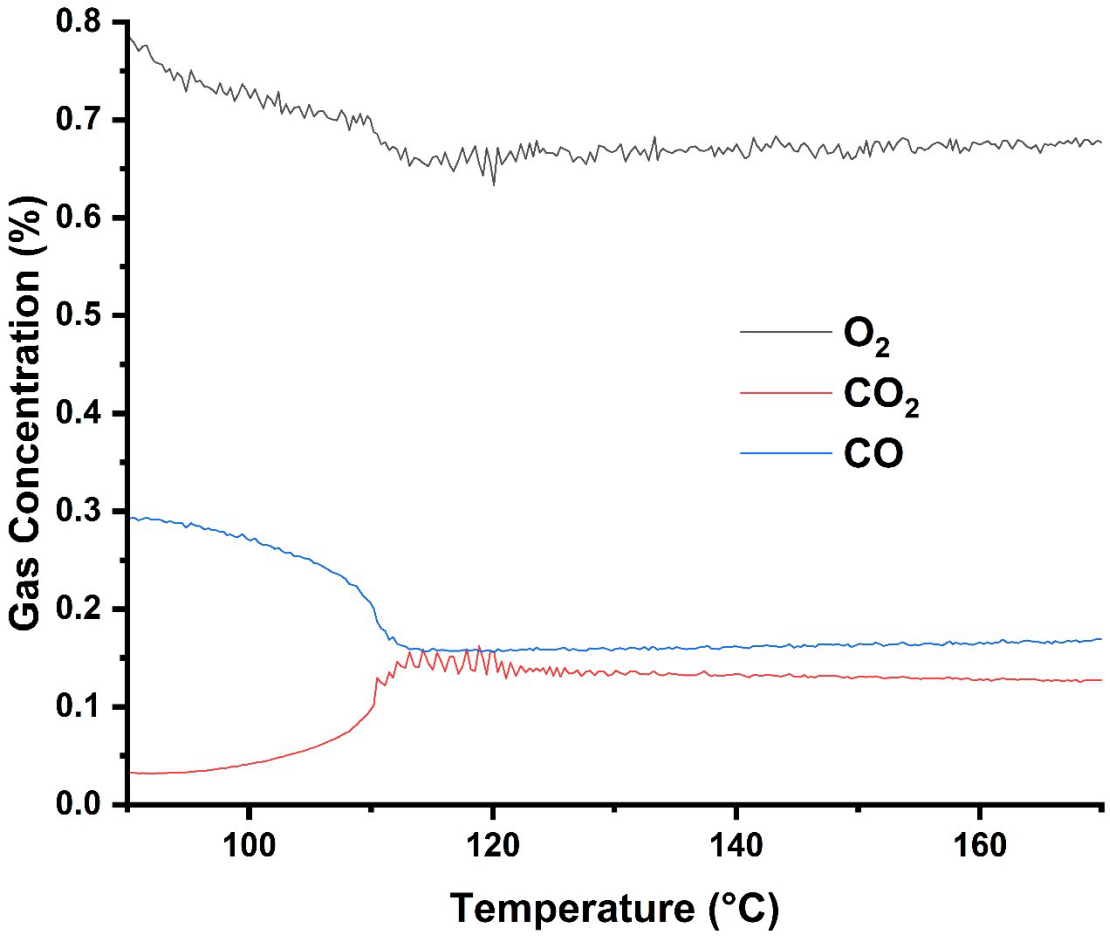

Supplementary Figure 41. Percentage mass concentration for CO, O_2 and CO_2 (m/z 28, 32 and 44 respectively) obtained through mass spectrometry during CO reaction on Rh/Al_2O_3, diluted 1:10 in SiC, as function of temperature.

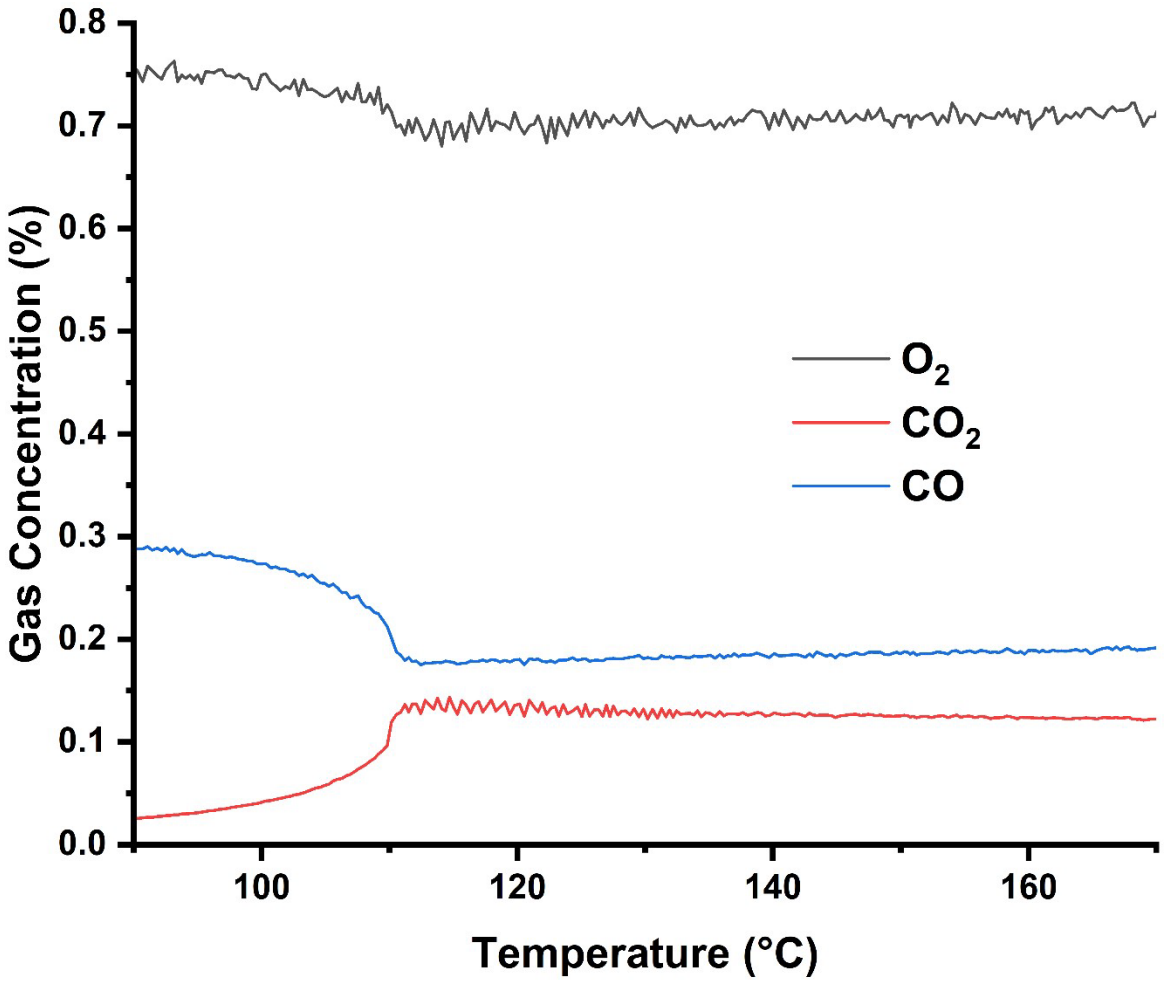

Supplementary Figure 42. Percentage mass concentration for CO, O_2 and CO_2 (m/z 28, 32 and 44 respectively) obtained through mass spectrometry during CO reaction on Rh/Al_2O_3, diluted 1:20 in SiC, as function of temperature.

`

Supplementary References

1. Swart, J. C. W., Van Helden, P. & Van Steen, E. Surface energy estimation of catalytically relevant fcc transition metals using DFT calculations on nanorods. *Journal of Physical Chemistry C* **111**, 4998–5005 (2007).

2. Ravel, B. & Newville, M. Athena, artemis, hephaestus: data analysis for x-ray absorption spectroscopy using IFEFFIT. *J. Synchrotron Rad.* **12**, 537 (2005).

3. Newville, M. IFEFFIT: interactive XAFS analysis and FEFF fitting. *J Synchrotron Radiat* **8**, 322 (2001).

4. Camp, C. H. pyMCR: A python library for multivariate curve resolution analysis with alternating regression (MCR AR). *J. Res. Natl. Inst. Radiat*. **124**, 124018 (2019).

5. Windig , W. et al. A new approach for interactive self modeling mixture analysis. *Chemometr. Intell. Lab. Syst.* **77**, 85 (2005).